CFD Modeling of Bi-Directional PMD inside Cryogenic Propellant Tanks Onboard Parabolic Flights

Jason Hartwig[*]

NASA Glenn Research Center, Cleveland, OH, 44135

Narottama Esser[†]

University of Florida, Gainesville, FL, 32611

Shreykumar Jain[‡]

Georgia Tech, Atlanta, GA, 30332

David Souders[§]

Flow Science Inc., Santa Fe, NM, 87505

Allen Prasad Varghese[**], Angelo Tafuni[††]

New Jersey Institute of Technology, Newark, NJ, 07102

Future cryogenic propulsion systems will require efficient methods with which to transfer cryogenic propellants from a depot storage tank to a customer receiver tank to minimize cost and maximize reusability. The Reduced Gravity Cryogenic Transfer project is currently developing advanced cryogenic fluid management technology and developing and validating new numerical models for three phases of transfer: line chilldown, tank chilldown, and tank fill. Additionally, multiple liquid nitrogen (LN_2) parabolic flight transfer rigs are being designed by universities and NASA to investigate the gravitational sensitivities that exist in

---

[*]Research Aerospace Engineer, Fluids and Cryogenics Branch, 21000 Brookpark Road, Cleveland, OH, 44135, AIAA Associate Fellow

[†]Graduate Student, Mechanical and Aerospace Engineering, Gainesville, FL, 32611

[‡]Graduate Student, Aerospace Engineering, North Ave NW, Atlanta, GA, 30332

[§]Senior Engineer, 683 Harkle Road. Santa Fe, NM, 87505

[**]Graduate Student, School of Applied Engineering and Technology, 323 Dr Martin Luther King Jr Blvd, Newark, NJ, 07102

[††]Assistant Professor, School of Applied Engineering and Technology, 323 Dr Martin Luther King Jr Blvd, Newark, NJ, 07102

Conference paper and presentation: Hartwig, J.W., Esser, N., Jain, S., Souders, D., Prasad Varghese, A., and Tafuni, A. “CFD Design and Analysis of a Perforated Plate for the Control of Cryogenic Flow under Reduced Gravity” AIAA-2023-0133, 2023 AIAA SciTech, National Harbor, MD, January 23 – 27, 2023.

these three technologies. In order to maximize the collection of low-g data during flights, it is required to extract as much LN_2 as possible from the supply tank, despite variable gravity levels. The purpose of this paper is to present computational fluid dynamics (CFD) volume of fluid simulations of LN_2 behavior in the supply tank onboard parabolic flights to validate the optimal design of a bi-directional propellant management device (PMD) using the commercial software FLOW-3D. A parametric study is conducted on the effects of gravity level, fill level, pore size, open area, thickness, and type of baffle on PMD performance. Based on results, the PMD as designed exceeds the targeted expulsion efficiency.

Nomenclature

$A_{x,y,z}$	=	Fractional Open Area
A	=	Pressure loss linear drag coefficient [1/s]
a	=	Acceleration [m/s^2]
B	=	Pressure loss quadratic drag coefficient [1/m]
$b_{x,y,z}$	=	Porous media flow loss accelerations [m/s^2]
Cp,Cv	=	Vapor specific heats [J/kg*K]
D_P	=	Pore diameter [m]
EE	=	Expulsion efficiency
$f_{x,y,z}$	=	Viscous Accelerations [m/s^2]
$G_{x,y,z}$	=	Body accelerations [m/s^2]
h	=	Height [m]
P	=	Pressure [Pa]
R_{DIF}	=	Turbulent diffusion source [kg/m^{3}s]
R_{SOR}	=	Mass source [kg/m^{3}s]
T	=	Temperature [K]
u	=	Flow velocity in x-direction [m/s]
u_{bulk}	=	Bulk velocity of fluid through plate [m/s]
V	=	Volume [m^3]

V_{tank} = Volume of tank [m^3]

$V_{residuals}$ = Volume of residual propellant [m^3]

V_F = Fractional open volume

v = Flow velocity in y-direction [m/s]

w = Flow velocity in z-direction [m/s]

φ = Porosity of plate

μ = Dynamic viscosity [Pa*s]

ρ = Density [kg/m^3]

γ = Vapor specific heat ratio

γ_{LV} = Surface tension [N/m]

I. Introduction

Future cryogenic propulsion systems will require efficient methods with which to transfer cryogenic propellants. Likewise, cryogenic fluid management technology development will be critical for future missions to the Moon, Mars, and beyond. Cryogenic propellants provide higher specific impulse over storable propellants, and thus will be widely used for missions involving space architectures such as Mars Ascent/Descent vehicles, nuclear thermal propulsion vehicles, and fuel depots. The last example, cryogenic propellant transfer depots (defined as an Earth-orbiting cryogenic propellant storage system) will be needed to support deep space missions because they will increase payload mass capability by allowing vehicles to refuel on the way to the Moon and beyond. These propellant depots will require transfer of cryogenic propellants that are characterized by low normal boiling point and surface tension. Thus, excessive boiloff issues and complex two-phase flow dynamics can result.

Since these space architectures will be subject to forces during launch or in orbit, the complex flow dynamics could result in vapor ingestion at the supply tank outlet port before all the liquid has been drained from the tank. In the case of a launch vehicle, additional propellant mass may be required, which increases the vehicle system mass and thus reduces the payload mass; vapor ingestion can cause the engine to stall or malfunction, resulting in failure. In the case of the propellant transfer depot, the surplus propellant mass directly reduces the depot transfer efficiency; acquiring single-phase liquid outflow from the supply tank is critical because vapor ingestion can lower the final liquid fill fraction in the customer receiver tank. Therefore, minimizing the surplus propellant mass through an efficient supply tank design is beneficial in terms of improving performance.

The easiest way to ensure single phase liquid outflow while in microgravity is to perform a settling thrusting maneuver; this, however, relies on consuming propellant. Classically, passive devices known as propellant management devices (PMDs) are used to favorably position liquid over the tank outlet. The purpose of a PMD is to separate liquid and gas phases within a propellant tank and to transfer vapor-free propellant from a storage tank to a transfer line en route to either an engine or receiver tank (depot application), in any gravitational or thermal environment [1]. While most PMD types have flight heritage with storable propellants, they have limited flight heritage with cryogenic propellants to-date. PMDs come in numerous styles and designs, each with its own specific purpose. Multiple PMDs are often required to meet the demands of a particular mission, whether using storable or cryogenic propellants. PMD performance is determined by three primary characteristics: PMD system mass, demand mass flow rate, and expulsion efficiency *EE*:

$$EE = 1 - \frac{V_{residuals}}{V_{\mathrm{tank}}} \quad (1)$$

Therefore, EE is a measure of how much of the tank is drained through the PMD before the PMD breaks down and ingests gas. For a detailed review of PMD physics as well as historical references, the reader is referred to [1, 2].

Acquiring data and developing accurate modeling of the complex heat transfer and fluid flow during the in-space propellant storage and transfer process is vital to enable or enhance these architectures and is thus critical towards design of these future systems using cryogenic propellants. Of all the variables, gravitational level is by far the hardest to simulate in near-terrestrial environments. While various platforms exist to acquire data for simulant fluids, options are limited for acquiring reduced gravity cryogenic data needed to investigate phenomena such as boiling, condensation, evaporation, sloshing, and pressurization, all of which are gravity-dependent phenomena.

The purpose of this paper is to present Volume of Fluid (VOF) Computational Fluid Dynamics (CFD) simulations of the supply tank cryogenic fluid behavior onboard a parabolic flight to validate the optimal design of a bi-directional PMD that will be used on various cryogenic parabolic flight experiments. A parametric study is conducted on the effects of gravity level, fill level, pore size, open area percentage, thickness, and type of baffle on PMD performance. The outline of the paper is as follows: First a background is given on the parabolic flight and on the CFD software FLOW-3D. Next, the problem description is presented, along with governing equations, boundary and initial conditions, and model settings. Then results are presented for the CFD simulation cases. Finally, conclusions and design recommendations are given.

II. Background

A. Parabolic Flight Cryogenic Experiments

All phases of in-space cryogenic propellant transfer are gravity dependent, including pressurization, PMDs, line chilldown, and tank chilldown and transfer. Most of the sub-processes involved are also gravity dependent, such as sloshing, boiling, condensation, and evaporation. While there are multiple instances of storable propellant transfer flight heritage, the transfer of cryogenic propellants has never been performed in an unsettled, microgravity environment. At the time of this publication, there is some quantitative reduced gravity line chilldown data in the open literature [3-5] but no tank chilldown or tank fill data in reduced gravity. Likewise, the only flight heritage for cryogenic PMDs is the Russian Buran and superfluid helium experiment [1].

The need to perform a carefully controlled, well-instrumented cryogenic fluid management (CFM) demonstration in Low Earth Orbit to obtain necessary data to enhance CFM technology as well as validate models is not a new concept. Despite the rich history of CFM ground testing and obvious need for a low gravity cryogenic storage and transfer test, achieving a CFM demonstration in a sustained low gravity environment remains as the elusive next step toward enabling multiple future in-space cryogenic propellant-based architectures [1]. While the ultimate goal is to perform a cryogenic flight experiment in a sustained, microgravity environment, there are other reduced gravity platforms that are essential for obtaining reduced gravity propellant transfer data at a more affordable cost (relative to a free flyer). These platforms include drop towers, parabolic flights, and suborbital flights. There are pros and cons to each platform from a science perspective. All platforms offer quick turnaround and affordable cost relative to ISS experiments or free-flying demonstrations. To contrast, for example, drop towers can achieve 10^{-5} g but the allowable volume is relatively small and the low gravity portion is milli-seconds to a few seconds. Suborbital flights can achieve 10^{-3}g for several minutes. While not opposed to flying cryogens, no United States suborbital provider presently allows venting gas overboard, implying that one must accumulate any vented gases from the experiment if flying cryogenic nitrogen, severely limiting the size of the test article. Meanwhile, parabolic flights have generous size, weight, and power availability, offer 25-30 parabolas per flight, and allow venting overboard. Because of these reasons, parabolic flights onboard the ZeroG [6] aircraft are currently one of the preferred options for small-to-medium scale payloads that can be used to investigate various gravity-dependent cryogenic propellant storage and transfer phenomena.

Multiple unique liquid nitrogen (LN_2) parabolic flight transfer rigs are being designed by various institutions and universities in collaboration with NASA Glenn Research Center to investigate the gravitational sensitivities that exist in various aspects of cryogenic propellant transfer. Regardless of the specific phenomena to be studied, in order to maximize the collection of low-g data during parabolic flights, it is required to extract as much LN_2 as possible from the supply tank, despite variable and changing gravity levels. During hyper-gravity or high-g phases of the mission, gravity forces the heavier liquid to the bottom of the tank and lighter gas to the top of the tank. Single-phase liquid extraction is straightforward with a liquid withdraw port or tube at the bottom of the tank. In the microgravity phases of the mission however, surface tension forces dominate, causing the liquid to slowly creep up the tank walls away from the outlet.

Therefore, to maximize data collection, the supply tank design should be optimized to reduce surplus propellant mass through delaying vapor ingestion at the outlet port. Because of the parabolic flight gravitational conditions and various outflow demand situations, a computational model is needed to study propellant outflow at these various conditions. The initial and boundary conditions that closely match the actual physical situation are needed for accurate predictions using CFD. The model predictions can then be used to understand flow dynamics in various phases of the mission and to design a robust PMD that can maintain single-phase outflow despite the two-way gravitational profile.

Therefore, the focus of this paper is to develop a CFD model to simulate propellant tank outflow under non-inertial forces typically experienced during a parabolic flight and use the results to determine the PMD design that will promise a minimum expulsion efficiency of 80% with a goal/target value of >90%. To the author's knowledge, no one has conducted this study before, nor have they designed a PMD to maximize expulsion efficiency for a cryogenic propellant tank during a parabolic flight. While the design presented is for a specific tank size, the geometry of the PMD can easily be scaled up or down to meet demands for a different tank.

Analysis performed in the current work falls under the Reduced Gravity Cryogenic Transfer (RGCT) project at NASA whose goals are (1) to investigate efficient cryogenic chilldown and transfer methods in a reduced gravity environment to enable future flight transfer systems, and (2) to develop and validate models for line chilldown, tank chilldown, and tank fill operations in 1-g and reduced gravity. RGCT is producing direct-cryogenic data anchored propellant transfer models at multiple levels, including zeroth order design models [7], fundamental boiling heat transfer and pressure drop correlations to be implemented into lumped capacitance codes [8-10], design tools for cryogenic tank chilldown and fill injection methods, including thermodynamic vent systems (TVS)-augmented injectors, development and validation of lumped capacitance codes Thermal Desktop [11] and the Generalized Fluid System Simulation Program (GFSSP) for tank chilldown and tank fill [12, 13], and CFD of tank chilldown using FLUENT [14]. CFD analysis presented in the current work uses FLOW-3D. What follows is a brief history of related FLOW-3D applications.

B. FLOW-3D Software History and Application

FLOW-3D [15] was selected to develop the CFD model used here to simulate cryogenic propellant tank outflow for these parabolic flight experiments primarily due to rich heritage in modeling free surface flows and sloshing. FLOW-3D has been extensively used to simulate fuel sloshing dynamics and analyze PMDs for operation in microgravity. For example, [16] and [17] used FLOW-3D to study liquid propellant sloshing in maneuvering spacecraft. Navickas et al. (1986) [18] used FLOW-3D to determine acceptable acceleration inputs to cause propellant settling for engine restarts in microgravity. Martin (1987) [19] studied propellant sloshing during zero-g separation of large propellant-filled vehicles such as Centaur from Space Shuttle. Der (1987) [20] studied ullage bubble deformation, breakup, and reorientation in liquid propellant tanks in low gravity. Fisher et al. (1991) [21] utilized FLOW-3D in the study of supply tank liquid hydrogen flow dynamics for space operations such as engine restarts and fluid transfer. Sasmal et al. (1991) [22] used FLOW-3D towards optimization of slush hydrogen storage tank pressurization process which occurs prior to engine ignition. Letourneur et al. (1993) [23] used FLOW-3D to study the effects of propellant sloshing on spin-up of the upper cryotechnic stage of Ariane V. Grayson et al. (1993) [24] used FLOW-3D to determine a propellant tank design concept incorporating PMDs for liquid-oxygen propellant outflow during vertical takeoff and vertical landing trajectory. Figus et al. (2000) [25] studied propellant motion inside a tank incorporating a PMD under neutral buoyancy using FLOW-3D, a technique used for station-keeping maneuvers of in-orbit spacecraft. Grayson et al. (2006) [26] later used FLOW-3D to study self-pressurization of the Saturn-S-IV-B LH_2 tank in a low-gravity environment of Earth orbit. Navickas and Cheng [27] used FLOW-3D to study oxygen and hydrogen sloshing behavior caused due to dynamic disturbances in a single-stage-to-orbit trajectory. Bakkum et al. (2010) [28] studied propellant sloshing in Orion Service Module propellant tanks under Martian and Lunar gravity with FLOW-3D. Behruzi et al. (2013) [29] used FLOW-3D to study cryogenic propellant management for cryogenic upper stages in tank heating and depressurization phases. Gaulke and Dreyer (2015) [30] studied the effects of perforated plate geometry on the capillary transport process of propellant between parallel perforated plates using

FLOW-3D simulations. Konopka et al. (2016) [31] used FLOW-3D to study LN_2 sloshing and drain behavior for cryogenic upper stage tank applications. Manning et al. (2019) [32] used FLOW-3D to study NTO and MMH propellant sloshing during high-g settling burns of the Europa Clipper spacecraft incorporating PMDs.

Essentially, these past studies demonstrate the benefits of employing FLOW-3D for modeling tank fluid sloshing and free surface flows in low gravity applications. FLOW-3D provides an accurate free surface solver utilizing the VOF method. The accurate tracking of the physics at the free surface is critical for cryogenic propulsion systems and propellant management applications because of the sloshing dynamics under microgravity and the use of PMDs for propellant acquisition. Therefore, FLOW-3D was chosen for the CFD simulations in this paper.

III. Problem Description

A. Problem Statement

As mentioned earlier, the purpose of this paper is to model cryogenic propellant tank fluid dynamics and outflow during a parabolic flight and to design an optimal PMD to ensure high expulsion efficiency during the worst-case acceleration profiles. As stated previously, NASA Glenn Research Center is partnering with multiple universities to design, build, and test cryogenic payloads in reduced gravity to obtain data on various aspects of cryogenic propellant transfer. As of writing this paper, the four most recent examples include: (1) a payload to gather flow boiling heat transfer coefficients and flow visualization for cryogenic liquids with Purdue University, (2) a payload to gather nucleation site density, bubble growth, and bubble departure diameter for cryogenic liquids with Massachusetts Institute of Technology, (3) a payload to study the effect of pulse flow and internal low-thermally conductive coating on transfer line chilldown with the University of Florida [5], and (4) a payload to study normal and subsurface pressurization for both autogenous and non-condensable pressurization schemes with the Aerospace Corporation. Subsequent publications will detail the experimental setup and results. These experiments have large storage dewars, relatively high flow capacity, and require single phase liquid extraction from the supply tank during all phases of the flight, and will thus benefit from a PMD used to acquire the majority of the liquid during low and hyper gravity.

Parabolic flights provide approximately 25-30 parabolas and generally follow a smooth flight profile as the airplane traverses low to hyper gravity conditions as shown notionally in Figure 1. During such nominal flights, the maximum anticipated upward gravitational acceleration is typically 0.190 m/s^2. Occasionally, and sometimes randomly or sporadically due to a variety of reasons (ex. inclement weather, uncontrollable changes in wind, etc.), higher-than-expected upward gravitational acceleration is experienced, which can reach as high as 0.805 m/s^2, over four times the nominal case. This latter case is plotted in Figure 2 from a previous flight. Vapor ingestion is more likely to occur during the higher magnitude gravity and therefore the gravity level at which these CFD simulations will be run is 1.0 m/s^2 worst-case. Later in the paper, the need for a PMD to prevent vapor ingestion at higher gravity levels will be clearly shown.

A cross-sectional view of the internals of the propellant tank used for this study is shown in Figure 3. Note that the tank is bolted or strapped down to the floor of the aircraft, therefore the forces on the tank are approximately same forces on the fluid inside the tank. The aluminum tank is vacuum jacketed (VJ) with an internal volume of approximately 195 liters, an end-to-end height of 0.9 m, and a diameter of 0.55 meters. Liquid is withdrawn from a central mounted dip tube from the bottom of the tank. The initial PMD design employed a circular porous plate and ring baffle as shown; later PMD designs also looked at replacing the ring baffle with another porous plate. The tank begins with 95% liquid level prior to expulsion, and since the tank is VJ, heat transfer between the tank and internal fluid was minimal. The tank is pressurized with either gaseous helium or gaseous nitrogen that is pre-conditioned to LN_2 temperatures below 85K to minimize the heat transfer between the pressurant gas and liquid. LN_2 begins in a saturated state near ambient pressure and the tank is pressurized as high as 689 kPa. This leads to a margin of over 340 kPa in pressure before cavitation through the porous element. As the experiment evolves, pressurant gas forces the liquid to be expelled via the dip tube. For the aforementioned flight experiments, liquid will need to be acquired during both low gravity and hyper-gravity conditions, since liquid demand is either only during low-g or continuous over both low and hyper gravity.

The primary design parameters for this study are the gravitational profile, liquid fill level, height, thickness, porosity, and pore size of the bottom porous plate, and the size of the ring baffle in first design iteration, or the upper porous plate characteristics in the later design iteration. Isothermal simulations (i.e. no heat transfer between fluid and void, and between fluid and solid components) were performed because the pressurant gas was cold-sinked to the tank and because the heat leak was minimal into the VJ storage dewar.

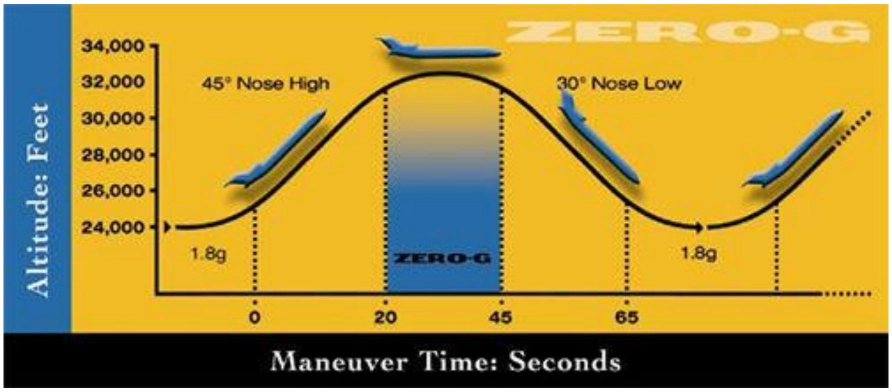

Figure 1: Nominal Flight Trajectory during a Parabolic Flight from [6]

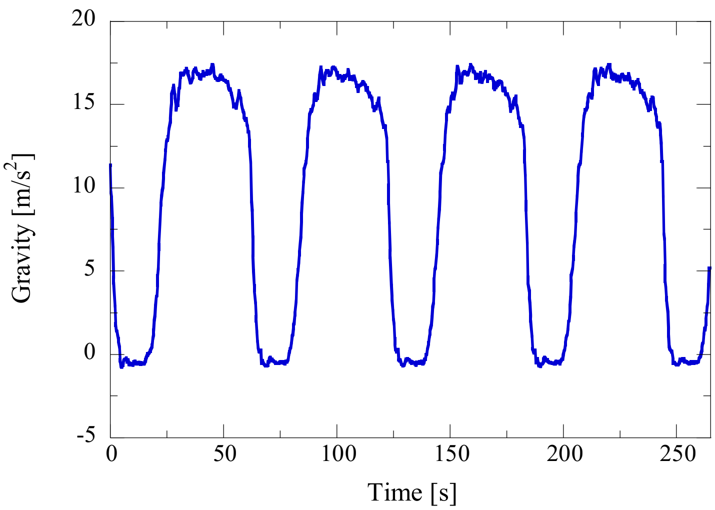

Figure 2: Worst-Case Parabolic Flight Gravity Data

B. Pore Size Selection

Given the above requirements, it is necessary to have at minimum one bi-directional perforated plate in the supply dewar as shown in Figure 3. The purpose of the plate is to ensure single phase liquid communication with the dip tube during all phases of the flight by (1) providing enough resistance to upward liquid flow during the low-g portions of flight and (2) by allowing liquid to drain back down below the plate (refilling the reservoir) during hyper gravity portions. Using the capillary bubble point pressure derived in [1], this relationship can be described as follows:

$$\rho a_{up} h_{plate} \leq \frac{4\gamma_{LV}}{D_P} \leq \rho a_{down} h_{LL,\min} \tag{2}$$

Using a worst-case upward acceleration of 1.0 m/s^2, a height of the plate of 0.1 m, and a residual liquid height of 0.64 cm ($h_{LL,min}$), the largest allowable pore diameter to block upward flow is ~420 microns, while the smallest allowable pore diameter to refill is ~380 microns. Therefore, to provide suitable resistance to upward motion while minimizing the residual liquid on top of the plate at breakdown, a suitable starting value for pore size of the perforated plate was chosen to be 400 microns. However, as the fluid drains from underneath the perforated plate there must be liquid communication from the top of the plate or else vapor ingestion will occur due to the outflow.

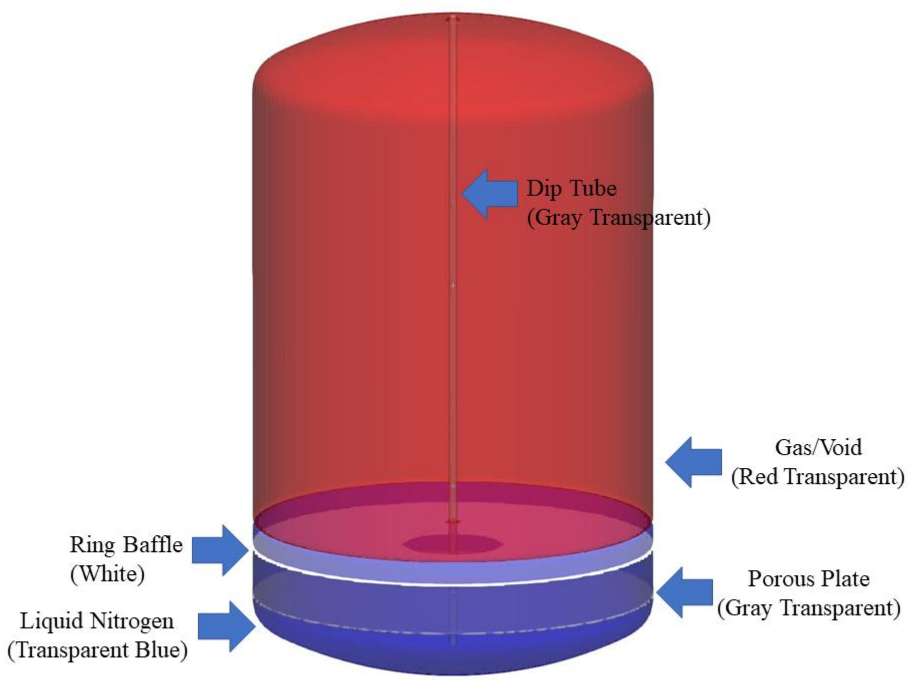

Figure 3: Propellant Tank and Tank Internals

C. Model Setup

FLOW-3D free surface tracking, one-fluid, with limited compressibility solver was used for all the cases performed in this study. It was determined early on that the two-fluid simulations would not be needed since the presence of gaseous helium would not impact design of the PMD due to the limited heat and mass transfer between ullage and liquid in the tank. Simulations were run using helium pressurant but not reported here for the sake of brevity. FLOW-3D's general mass continuity equation for a model in cartesian coordinate system is:

$$V_F \frac{\partial \rho}{\partial t} + \frac{\partial}{\partial x}\left(\rho u A_x\right) + \frac{\partial}{\partial y}\left(\rho v A_y\right) + \frac{\partial}{\partial z}\left(\rho w A_z\right) = R_{DIF} + R_{SOR} \qquad (3)$$

For isothermal simulations, density is assumed to be constant in time, and there is no mass source. The turbulent diffusion term is only used for turbulent mixing processes involving fluid with non-uniform density which does not apply to isothermal simulations here. Therefore, the mass continuity equation simplifies to:

$$\frac{\partial}{\partial x}\left(\rho u A_x\right)+\frac{\partial}{\partial y}\left(\rho v A_y\right)+\frac{\partial}{\partial z}\left(\rho w A_z\right)=0 \tag{4}$$

The general momentum equation, applied in three directions are as follows:

$$\frac{\partial u_j}{\partial t}+\frac{1}{V_F}u_k A_k\frac{\partial u_j}{\partial x_k}=-\frac{1}{\rho}\frac{\partial P}{\partial x_j}+G_j+f_j-b_j-\frac{R_{SOR}}{\rho V_F}\left(u_j-u_{j,s}\right) \tag{5}$$

For isothermal simulations, density is assumed to be constant and there is no mass source. Therefore, the momentum equation simplifies to:

$$\frac{\partial u_j}{\partial t}+\frac{1}{V_F}u_k A_k\frac{\partial u_j}{\partial x_k}=-\frac{1}{\rho}\frac{\partial P}{\partial x_j}+G_j+f_j-b_j \tag{6}$$

The fluid for this study is LN_2. The fluid material properties were input from REFPROP [33] which is a National Institute of Standards and Technology (NIST) database for thermophysical properties of fluids and fluid mixtures. The general model setup in FLOW-3D for all the simulations is described as follows.

1. **Global**

   Simulations were run as high as 689 kPa, but for most simulations, the reference pressure was set to 345 kPa (50 psia) and reference temperature was set to 80 K (saturation temperature at 138 kPa). These reference properties would be allocated to any unassigned pressure/temperature properties. Run time varied based on the desired outcome.

2. **Physics**

The free-surface tracking was activated along with one-fluid incompressible flow for all simulations. There were four physics models activated for all simulations. First, the Surface Tension model was activated with contact angle defined as zero because of complete wetting property of LN_2 [1]. The surface tension value was set to the value from Table 1. The second model activated was the Gravity and Non-Inertial Reference model, and the actual flight parabolic gravity data was fed into the model. The third model activated was the Viscosity and Turbulence model, tracked by the built-in Renormalized Group (RNG) model, and the fourth model was the Bubble and Phase Change model with the selection of Adiabatic Bubbles. The vapor specific heat ratio was set to 1.4 and default void initial pressure was set to 345 kPa. The default constant pressure bubbles assumption was invalid since vapor pressure is not constant in confined vapor regions that open up within the fluid. The Adiabatic Bubbles model evaluates the pressure in each confined void region based on the assumption of reversible adiabatic expansion/compression of perfect gas. The pressure is evaluated using the assumption of constant PV^{γ}, where V is the volume of void region and γ is the ratio of vapor specific heats, $\gamma = Cp/Cv$.

3. Fluids

For all simulations, the properties of LN_2 and liquid-vapor interface surface tension properties were input into the model here. Constant density, dynamic viscosity, and isothermal compressibility at 80K saturation temperature were input from REFPROP. Similarly, constant surface tension at 80K was input from the surface tension model from [1]. These inputs are summarized in Table 1.

Table 1: Liquid Nitrogen Properties Initialization for All Simulations

LN2 Property	Initial Value
Density [kg/m^3]	793.9
Dynamic Viscosity [µPa*s]	145.1
Isothermal Compressibility [1/Pa]	3.56E-09
Surface Tension [mN/m]	8.27

4. Geometry

The modeling approach for the tank design was to develop a solid Standard Triangle Language (STL) file of the tank cavity and import it into FLOW-3D as a complement object. In FLOW-3D, a complement geometry object adds solid material outside of the STL geometry up to the computational domain defined by mesh block boundaries. Therefore, the tank complement STL would essentially create a tank cavity. This was to avoid having to resolve the tank wall thickness which would impose a reduction on the mesh cell size and significantly increase the runtime beyond practicality. Once the tank cavity was defined, the dip tube was added as a solid cylindrical primitive object (primitive object means it can be created in FLOW-3D without any import files). Since fluid-to-solid heat transfer was not needed, the material for the geometry components did not affect results. Next, a primitive cylindrical hole object was used to create a blind hole at the inside top of the tank. A void pointer was placed in that hole to set the pressure in the tank throughout the simulation.

For the porous plate representation, a porous media geometry component was created using a cylindrical primitive object. Since the porous plate pore size was small, resolving the pores with the plate STL file would require the mesh cell size to be greatly reduced resulting in an exponential increase in runtime. Therefore, a porous media object was created to represent the perforated plate. The porous media model in FLOW-3D is implemented by applying volume averaged quantities to the porous region and calculating the bulk fluid velocity and pressure drop using whichever porous media drag model is selected, which in this case was the Forchheimer Saturated Drag Model [34]. The plate was placed at the 7.8% fill level height with the intent to hold liquid under the plate. The thickness of the plate was set to 0.3175 cm (1/8 in) initially although the thickness was varied for later cases due to structural concerns. Table 2 lists the plate thicknesses as well as all variable properties for the plate for the simulation cases ran. A mesh plane was placed at the 7.8% fill level height to ensure that the porous plate was properly represented in FLOW-3D. The pressure drop across the plate was modeled in FLOW-3D using the Forchheimer Saturated Drag Model which calculates the pressure drop through the plate as follows:

$$-\nabla P = A \cdot \left|u_{bulk}\right| \mu \frac{(1-\phi)^2}{\phi^3} + B \cdot \left|u_{bulk}\right|^2 \rho \frac{(1-\phi)}{\phi^3} \tag{7}$$

However, comparing this model with the accumulated cryogenic screen bubble point and pressure drop data indicated that this model was not accurately calculating the pressure drop. A custom user-defined function was then built to accurately predict the pressure drop across the screen for gas/liquid and liquid/liquid cases. For more information on how to ensure proper implementation of the flow-through-screen pressure drop in FLOW-3D, including how to enforce the capillary pressure and correct drag coefficients, the reader is referred to [1] or recommended to reach out to the authors.

5. Initial

The tank setup in FLOW-3D is shown in Figure 4 with fluid fraction and the meshing. Due to the way FLOW-3D displays the porous media geometry, the bottom porous plate is hardly visible but the discontinuity in the center dip tube indicates the height of the plate. To initialize the fluid, LN_2 was inserted into the tank using Fluid Regions with a primitive cylindrical object. A cylinder was created with its width extending past the tank cavity width to ensure full liquid coverage within the tank cavity (FLOW-3D does not insert fluid into the blocked solid cells despite the fluid cylinder extending into the solid region). The fill level percent for each simulation was calculated based on the internal volume of the tank being approximately 195L. The fluid fraction was set to 1 to represent single-phase liquid nitrogen. The initial pressure of void was set to 345 kPa.

Lastly, a void pointer was placed in the small hole at the top of the tank to set the tank pressure throughout the simulation to be 345 kPa. A void pointer only works to set the pressure in the tank when in contact with a void region so the pressure in the tank would vary somewhat when the fluid covered the pointer, but did not affect simulations.

6. Mesh

FLOW-3D uses a structured mesh as a simple and robust meshing method. The meshing for the computational domain was developed by creating a mesh block manually. The mesh block was defined to extend slightly beyond the tank cavity to capture the entire tank geometry while creating a solid domain outside the tank cavity. As previously mentioned, a mesh plane was also added at the 7.8% fill level height in the Z-direction to improve the meshing of the porous plate. A mesh plane was also added later at the 15.7% fill level height in the Z-direction for the cases where the ring baffle was replaced by a second porous plate. The mesh cell size chosen for the simulations was nominally 0.005 m after verifying with a grid convergence study. With that set mesh cell size, the total number of cells was approximately 2.9 million. Figure 4 shows the mesh grid overlay on the tank domain at the nominal grid size.

7. Boundaries

For all simulations, the mesh boundary conditions were all set to symmetry. These mesh boundaries were outside the tank cavity domain, therefore, symmetry boundary conditions were chosen because they do not apply any condition on the tank domain. Instead, the solid walls of the tank acted as the boundary conditions for the fluid inside the tank.

8. Numerics

For each simulation, the pressure convergence criterion was adjusted from its default value of 1 to various lower values no lower than 0.001 depending on which value allowed FLOW-3D to successfully run the simulation with no errors. Additionally, the lowest porosity value set for the porous plate designs was 0.0053 corresponding to the 0.63% open area case. The FAVOR EPS limit must be smaller than 0.0053 to avoid complete cell blockage at the plate. Therefore, the EPS limit was set to 0.005 to accurately resolve the lowest porosity design. This EPS limit of 0.005 was set for all simulations to maintain consistency in the simulations.

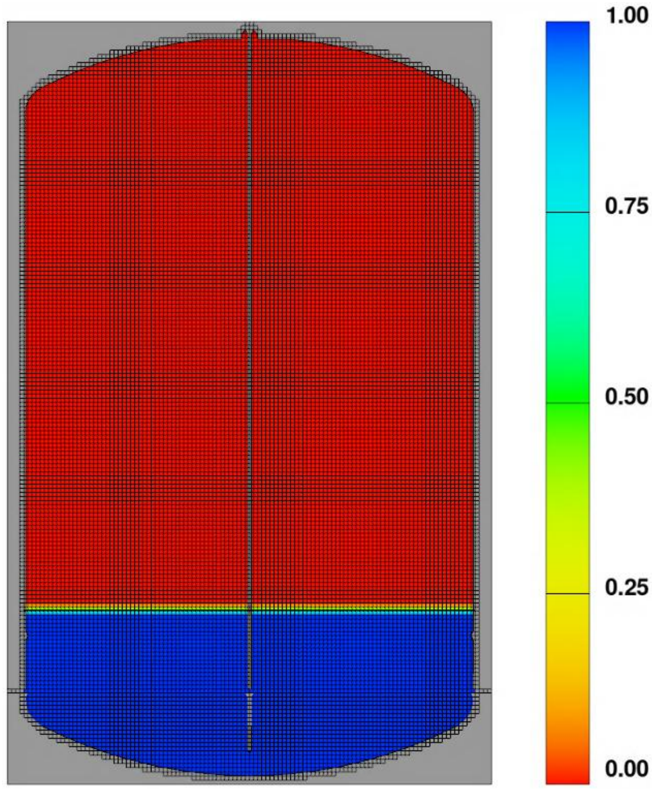

Figure 4: FLOW-3D Tank Layout with LN_2 Fluid Fraction and Grid Mesh

9. Baffles

For the ring baffle representation, a baffle object was created in FLOW-3D by defining it as a surface. This surface definition snaps to the nearest mesh grid lines and therefore does not affect the volume fraction of the cells. The ring baffle was defined by setting a Z height, which was set to the 15.7% fill level. The porosity was set to 0 so that the ring baffle was represented as a solid obstacle. Then the inner and outer radii of the baffle were defined to create the ring baffle shape. The inner radius is one of the design parameters of this study, while the outer radius was set to overlap with the tank walls so that there would be no gaps around the edges.

10. Sources

To represent outflow from the bottom of the tank, a mass/momentum source object was created, which introduces or removes fluid based on the specified geometry and flow rate. Based on the user-defined location, shape, and orientation, the FLOW-3D solver generates a uniform array of particles which introduces the fluid into the domain. The object can also be defined as a sink by inputting a negative flow rate, thus being able to extract the fluid out of the domain. Modeling source/sink with mass/momentum source objects is beneficial in cases of small source/sink (relative to the mesh cell size) because fluid can be added/removed without having to resolve the geometry of the object as was the situation in these simulations. There is another capability in FLOW-3D to create a mass source object, but the mass/momentum object was chosen because it can extract fluid without geometry representation and therefore does not create any unwanted solid space in the domain. The mass/momentum object was created as a circular face with the specific geometry defined to match the tank outlet. It was placed one mesh cell above the solid cells of the bottom of the tank just below the dip tube outlet to avoid any solid blockage of the sink from overlap with the tank solid structure. The mass/momentum sink is shown in Figure 5. The outflow could take any desired profile (e.g. outflow only during low-g or continuous outflow over low and hyper gravity). The outflow rate for all simulations was set to 0.15kg/s.

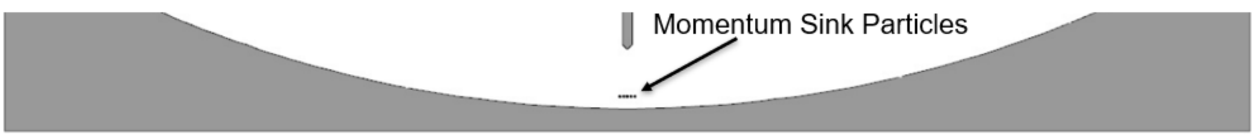

Figure 5: FLOW-3D Mass/Momentum Sink

11. Probes

To track the pressure drop across the porous plate, two probes were placed above and below the porous plate on two sides of the tank for a total of 4 probes. The probes were set to both have a height difference of 0.025 m so that hydrostatic pressure differences could be calculated as a function of time using the z-axis linear acceleration data from FLOW-3D. The hydrostatic pressure difference would then be subtracted from the average pressure differences measured by the probes to calculate the pressure drop across the plate.

12. Flux Surfaces

One small cylindrical flux surface was placed just above the mass/momentum sink to capture gas ingestion by looking at the fluid-filled area of the flux surface.

13. Sampling Volumes

A cylindrical sampling volume that encompassed the entire volume under the porous plate was created to monitor the fluid fraction under the porous plate to see if bubbles were ingested past the plate.

14. Output

For all simulations, data was gathered from the probes, flux surfaces, sampling volumes, and other data sources at a sampling rate of 0.1 seconds. Restart data, which included data for the 2D and 3D visualizations were set to output every 0.5 seconds.

D. Simulation Cases

Table 2 shows the test matrix of simulations. For the ring baffle size, R represents the inner radius of the cylindrical portion of the tank. The ring baffle size defines the inner radius of the ring baffle. For example, for an R/3 baffle, the open area is a circle located along the center line, with a radial distance of 0.183m. For an R/4 baffle, the open area is a circle with radius of 0.138 m. As shown in Table 2, two simulations were run with no PMD to show the need for the PMD, one at nominal or lower magnitude gravity, and one at the worst-case higher magnitude gravity. Next, several simulations were run with varying fill heights to determine at what fill level gas ingestion at the outlet was most likely to occur. Lastly, simulations were run with the varying design parameters to determine the PMD design with the highest expulsion efficiency.

Table 2: Test Matrix of Simulations

Simulation	Plate Open Area %	Plate Pore Size [μm]	Ring Baffle Size	Second Plate	Initial Fill Level	Plate Thickness [cm]	Other Conditions
Case 1	-	-	-	-	43.60%	-	No PMDs, Lower Magnitude Gravity
Case 2	-	-	-	-	99%	-	No PMDs, Worst-Case Gravity, 1.0 m/s/s max negative-g
Case 3	2.5	400	R/4	-	57.70%	0.3175	Worst-Case Gravity
Case 4	2.5	400	R/4	-	19.60%	0.3175	Worst-Case Gravity
Case 5	2.5	400	R/3	-	48.40%	0.3175	Worst-Case Gravity
Case 6	2.5	400	R/3	-	19.60%	0.3175	Worst-Case Gravity
Case 7	2.5	400	0.79R	-	43.60%	0.3175	Worst-Case Gravity
Case 8	2.5	800	R/4	-	19.60%	0.3175	Worst-Case Gravity
Case 9	0.63	400	R/4	-	19.60%	0.3175	Worst-Case Gravity
Case 10	0.63	400	-	Yes	17.00%	1.27	Worst-Case Gravity
Case 11	0.63	400	-	Yes	9.10%	1.27	Worst-Case Gravity
Case 12	0.63	400	-	Yes	13.30%	1.27	Worst-Case Gravity
Case 13	0.63	400	-	Yes	9.10%	0.953	Worst-Case Gravity

IV. Results and Discussion

Case 1 – No PMD, Lower Magnitude Gravity

For each case, the initial fluid snapshot is displayed with the visualization style shown in Figure 3. For the fluid snapshots after the initial snapshot, the same style was used but the viewing angle was adjusted to be orthogonal to the tank. For Case 1, critical snapshots of an orthogonal, 3D, semi-transparent view of the fluid in the tank as a function of time are shown in Figure 6. As shown, vapor ingestion at the outlet occurs at a relatively low fill level for the nominal magnitude gravity case at a point of 380 seconds past initialization. Figure 7 plots the volumetric flow rate out of the tank as a function of time and shows constant flow rate out up to the point of failure. Figure 7 also plots the fluid fraction of the outlet flux surface and clearly shows the vapor ingestion occurring at 380s as the flux surface fill fraction drops significantly. Figure 7 also plots the sampling volume fluid fraction and basically indicates that the fluid begins significant sloshing around 300s, with motion persisting until breakdown. These three curves are needed to determine the point of vapor ingestion and thus expulsion efficiency to compare with 3D visualization for all cases subsequently.

Based on 3D visualization and Figure 7, the expulsion efficiency was calculated to be 93% with no PMD at the nominal gravity level. Interestingly, the implication is that if the flight conditions were perfect every time, then it is possible to acquire the target 90% expulsion efficiency without a PMD. However, since there are so many factors that cannot be controlled which will lead to higher-than-expected upward accelerations, the PMD is certainly warranted to guarantee high expulsion efficiency with high margin in design. At worst, even if flight conditions are ideal, the PMD would allow a factor of safety of 4-5 in unwanted acceleration.

Case 2 – No PMD, Worst-Case Magnitude Gravity

Critical snapshots of the fluid in the tank as a function of time are shown in Figure 8 for Case 2. As shown, for this higher magnitude gravity case, vapor ingestion occurs during the very first upwards-g parabola. Figure 9 shows that the constant volumetric flow rate is interrupted at around 10 seconds, that the outlet flux surface fill fraction drops significantly at 10.4 seconds, and that the bubble remains at the bottom of the tank throughout the duration of the upwards-g parabola. Case 2 clearly indicates the need for a PMD to prevent vapor ingestion during any off-nominal gravity levels.

Case 3 – 2.5% Open Area, 400µm, R/4, 57.7% Initial Fill

Case 3 compares high fill level to low fill level for the baseline design, defined as a bottom porous plate with 2.5% open area, 400 micron pore size, and a top ring baffle with an R/4 opening under higher gravity. This case was run to compare with the lower fill level case to determine if gas ingestion would occur at the higher fill levels or only at lower fill levels. Therefore, an expulsion efficiency was not calculated here.

Figure 10 shows critical snapshots of the fluid configuration during the flight. As shown, during the low-g part of the parabolic flight, the bulk of the fluid moves to the top of the tank while the ring baffle and porous plate trap the remaining liquid below. As seen in Figure 11, the fluid drains at a constant rate except for some small volume errors causing slight variance, indicating that no gas is being ingested at the outlet. This conclusion is further supported by the flux surface fluid fraction in Figure 11, which shows that the outlet is covered by the liquid throughout the simulation. Lastly, it can be seen from Figure 10b that only a very small amount of vapor makes it under the porous plate for this specific case, not enough to cause vapor ingestion into the dip tube.

The average measured pressure drop from FLOW-3D for this case was 1.22 Pa while the calculated pressure drop for this case was 1.11 Pa, which shows that the pressure drop across the porous plate is accurately represented by the custom user defined function and FLOW-3D in this case. All other subsequent measured versus calculated pressure drops are summarized in Table 3.

Case 4 – 2.5% Open Area, 400µm, R/4, 19.6% Initial Fill

Case 4 compares the base case PMD design at low fill level with high fill level from Case 3. Figure 12 plots the fluid configuration at various times and shows that the porous plate and ring baffle traps some of the fluid while the remaining fluid moves upwards to the top of the tank at time = 15 seconds (Figure 12b). Vapor is then ingested in the dip tube during the low-g phase of the second parabola as shown in Figure 12e. Figure 13 seems to show a constant volumetric flow rate that does not seem to be affected by the small amount of vapor ingestion, and also shows that the outlet ingests gas at t=69.5 s because the fluid fraction of the outlet flux surface drops significantly. Figure 13 (fluid fraction of volume below the porous plate) also shows that some bubbles are ingested below the porous plate during the second parabola which can also be seen in Figures 12d and e. Initial vapor ingestion is seen both visually and from the 1D data at approximately the same time, thus the expulsion efficiency for this case is 87.4%.

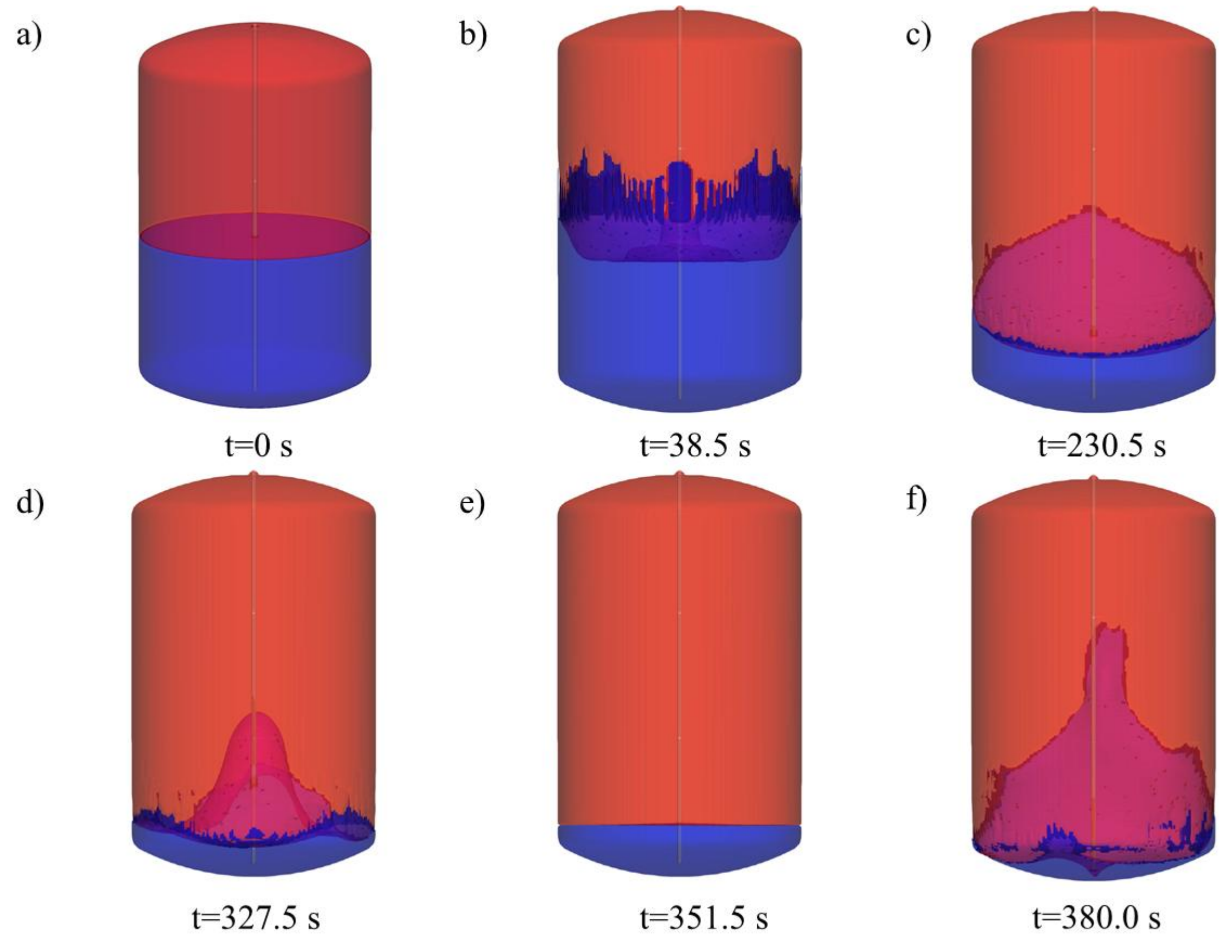

Figure 6: Visualization of Fluid for Case 1 for a) Initial Fill Level, b) Middle of First Upwards-G Parabola, c) Upwards-G Phase Halfway through Simulation, d) Second-to-Last Parabola, e) Fill Level Prior to Vapor Ingestion, and f) Point of Vapor Ingestion

Case 5 – 2.5% Open Area, 400µm, R/3, 48.4% Initial Fill

Case 5 compares an R/3 upper ring baffle PMD to the base case design R/4 upper ring baffle at high fill level from Case 3. Similar to Case 3, this case was run as a sanity check to ensure no vapor was ingested at high fill levels; no expulsion efficiency was calculated here. As in the previous cases, the fluid moves to the top of the tank while the porous plate and ring baffle traps the remainder of the fluid at the bottom of the tank during the low-g phase. It can be seen from Figure 14b, 14d, 14f and Figure 15 that little to no vapor makes it under the porous plate for the higher fill levels for several parabolas. Figure 15 shows the fluid drains at a constant rate except for some small volume errors causing slight variance, which indicates that no gas is being ingested at the outlet. This conclusion is further supported by the flux surface fluid fraction in Figure 15, which shows that the outlet is covered by liquid throughout the simulation.

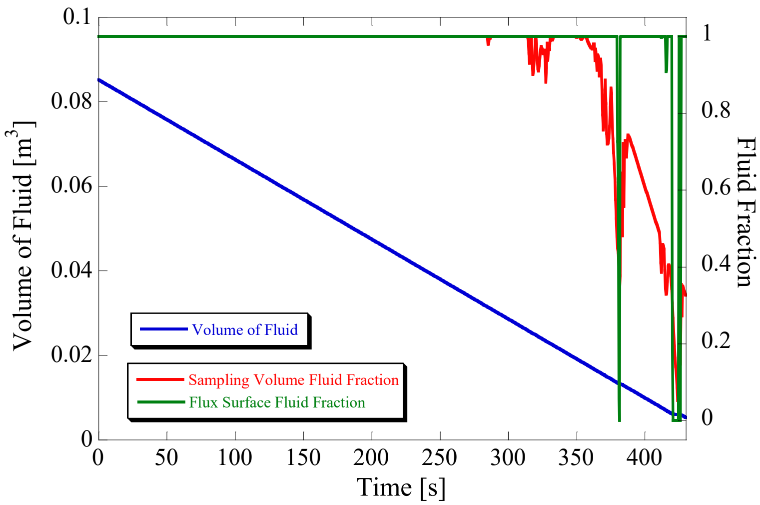

Figure 7: Case 1 – Volume of Fluid, Fluid Fraction of Outlet Flux Surface, and Fluid Fraction of Volume Below Porous Plate vs Time

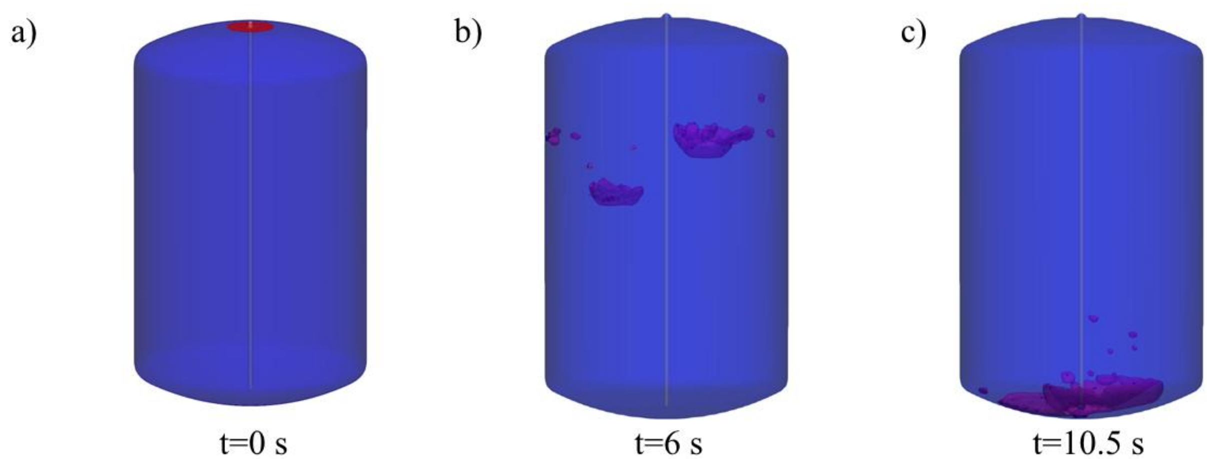

Figure 8: Visualization of Fluid for Case 2 for a) Initial Fill Level, b) Start of First Upwards-g Parabola, and c) Point of Vapor Ingestion

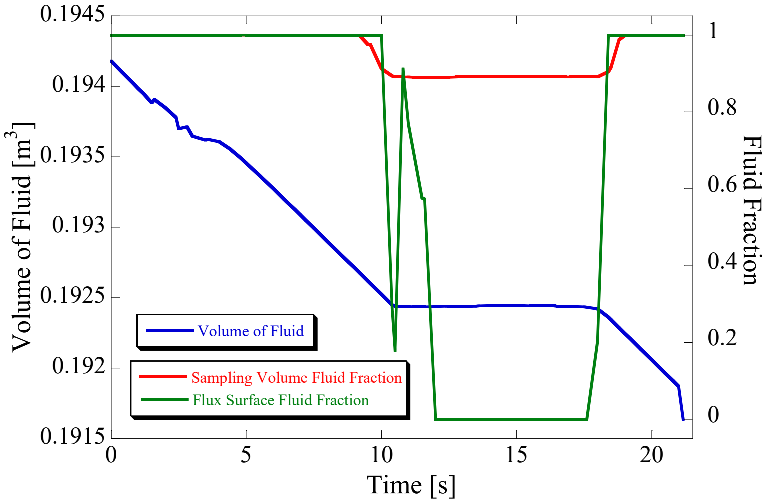

Figure 9: Case 3 – Volume of Fluid, Fluid Fraction of Outlet Flux Surface, and Fluid Fraction of Volume Below Porous Plate vs Time

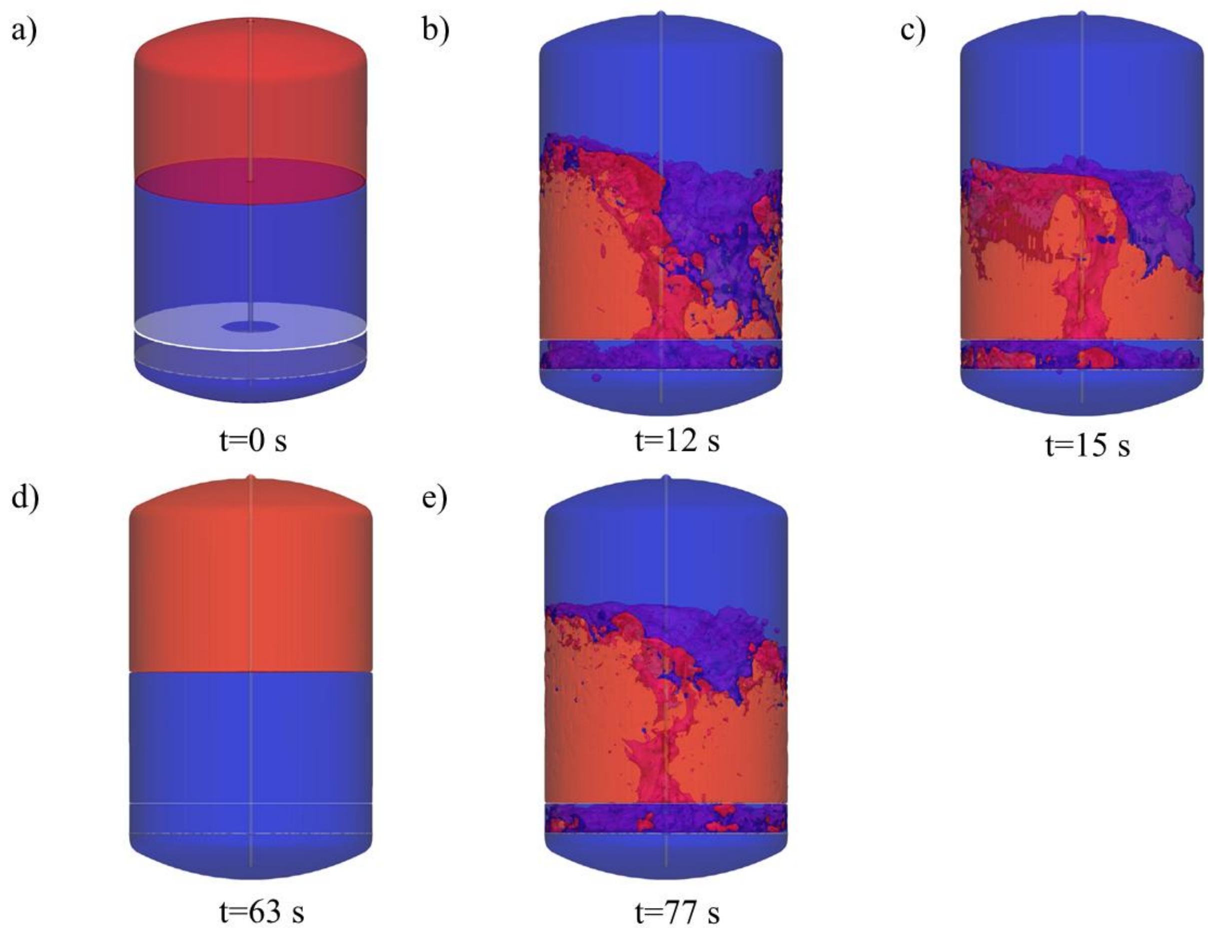

Figure 10: Visualization of Fluid for Case 3 for a) Initial Fill Level, b) First Bubble Ingestion Past Porous Plate, c) Middle of First Parabola, d) Second Upwards-g Parabola, and e) Middle of Second Parabola.

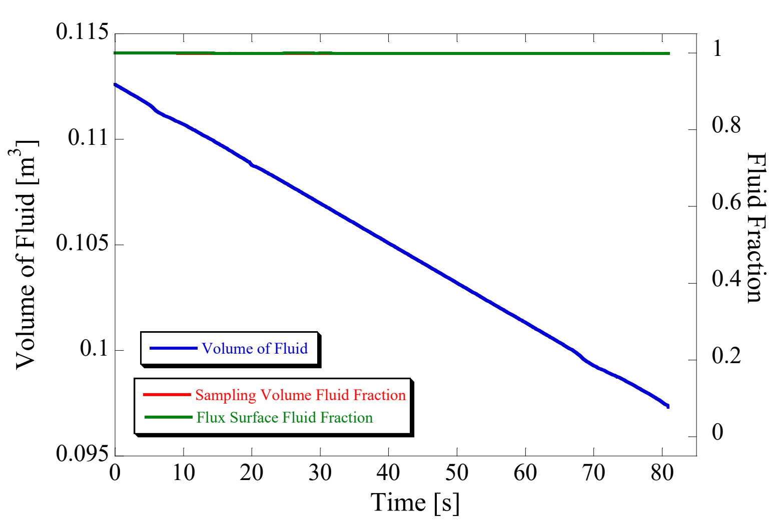

Figure 11: Case 3 – Volume of Fluid, Fluid Fraction of Outlet Flux Surface, and Fluid Fraction of Volume Below Porous Plate vs Time

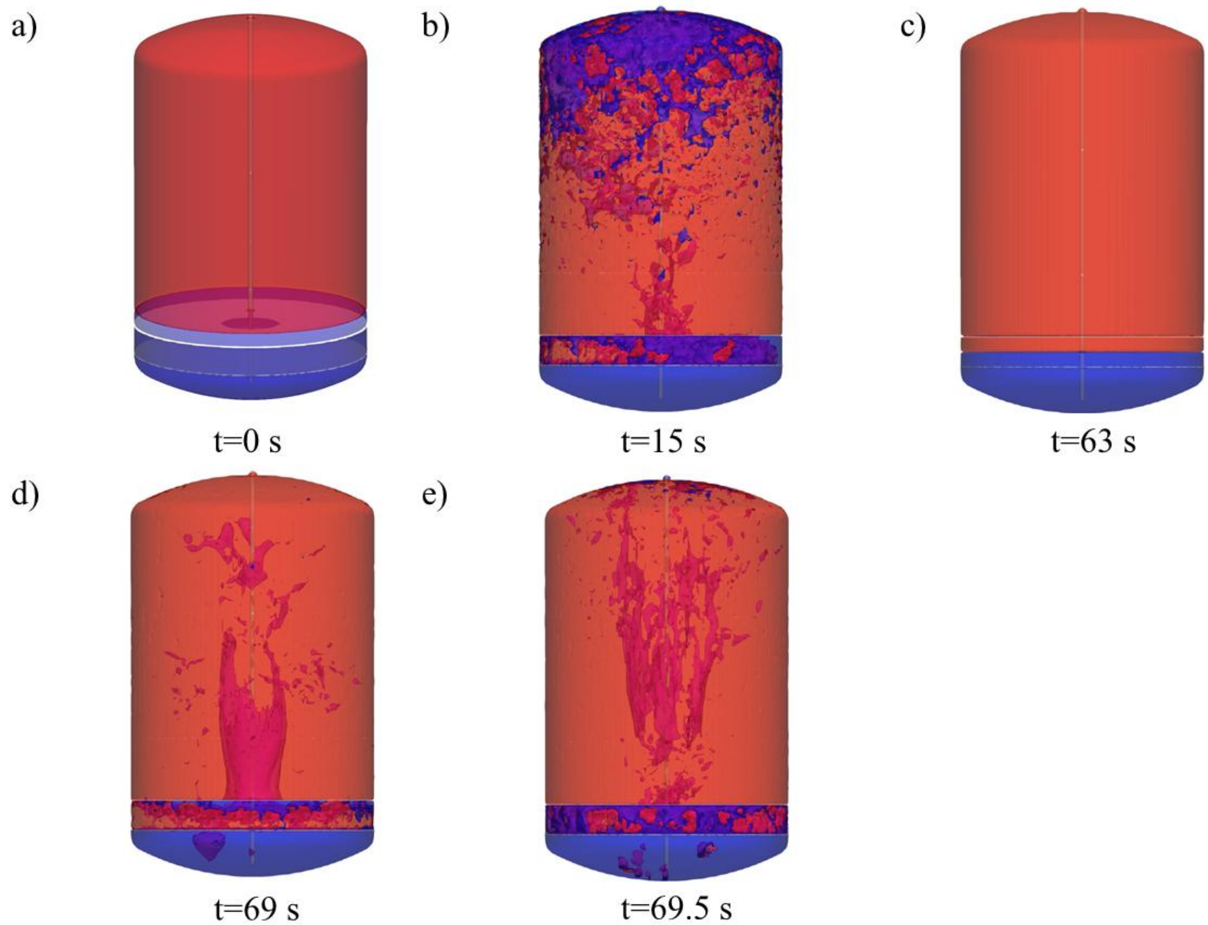

Figure 12: Visualization of Fluid in the Supply Tank as a Function of Time for Case 4 for a) Initial Fill level, b) Fluid Configuration during Middle of First Parabola, c) Initial Configuration before Second Upward-g Parabola, d) Instance of First Bubble Ingestion Past Porous Plate, and e) At the Point of Vapor Ingestion

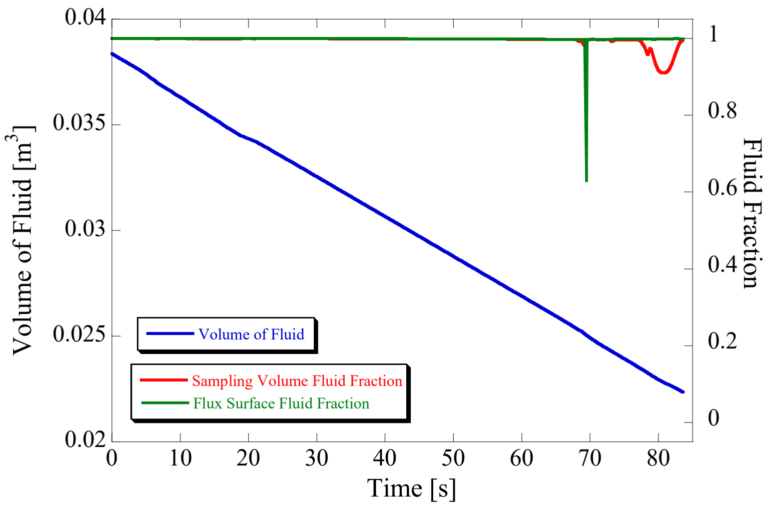

Figure 13: Case 4 – Volume of Fluid, Fluid Fraction of Outlet Flux Surface, and Fluid Fraction of Volume Below Porous Plate vs Time

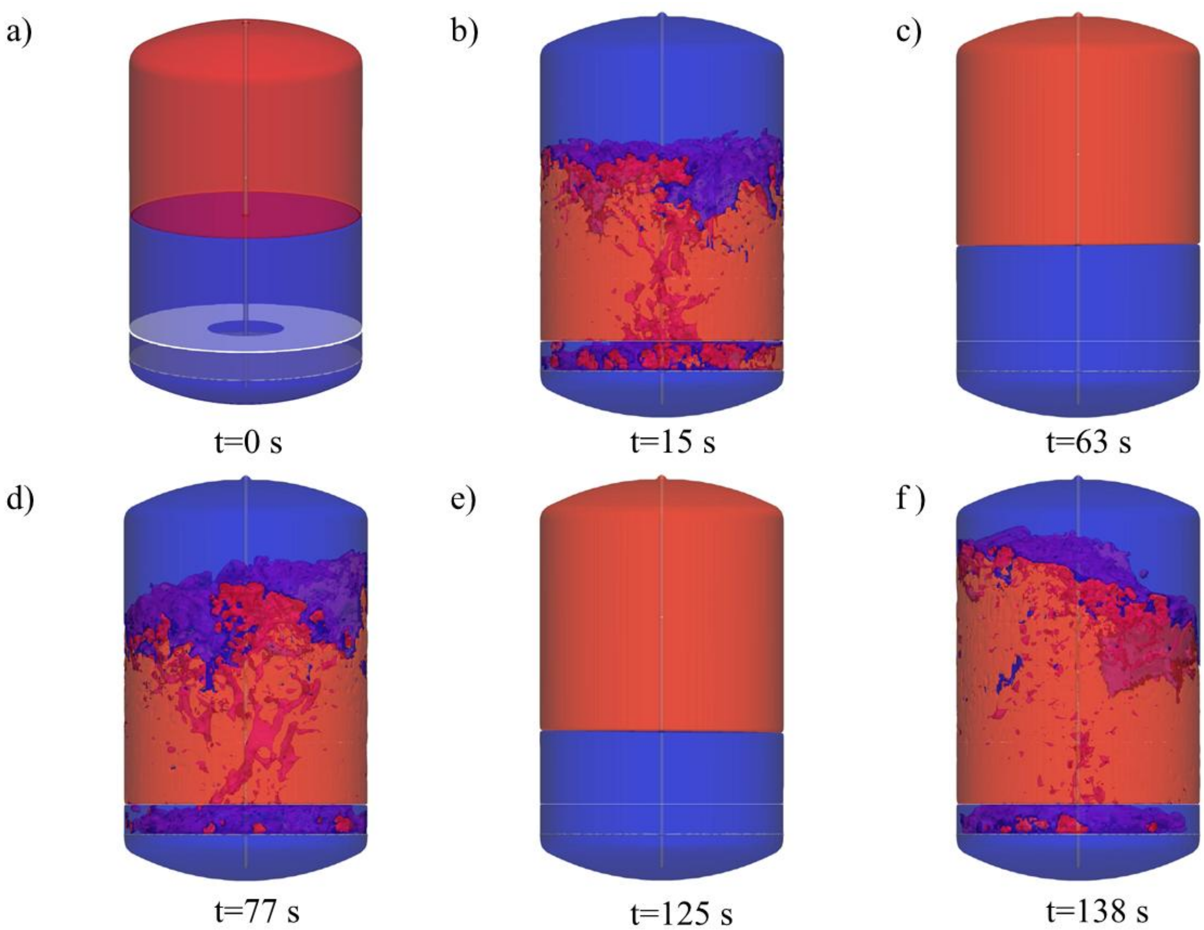

Figure 14: Visualization of Fluid for Case 5 a) Initial Fill level, b) Middle of First Parabola, c) Before Second Upward-g Parabola, d) Middle of Second Parabola, e) Before third Upwards-g Parabola, and f) Middle of Third Parabola

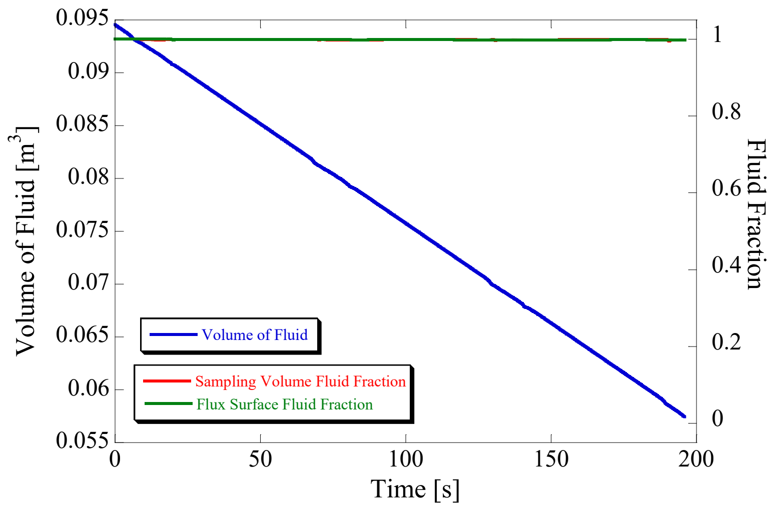

Figure 15: Case 5 – Volume of Fluid, Fluid Fraction of Outlet Flux Surface, and Fluid Fraction of Volume Below Porous Plate vs Time

Case 6 – 2.5% Open Area, 400µm, R/3, 19.6% Fill

Case 6 compares an R/3 upper ring baffle PMD to the base case design R/4 upper ring baffle at low fill level from Case 4. Similar to Case 4, this case was run to determine the expulsion efficiency and also if the R/3 upper baffle led to smaller residuals at breakdown. As in previous cases, Figure 16 shows that the porous plate and ring baffle traps some of the fluid while the remaining fluid moves upwards to the top of the tank during the first low-g phase. Figure 17 shows a constant flow rate up until t=128.0 s where the flow rate goes to zero due to gas being ingested. Figure 17 also shows that the outlet ingests gas at t=128.0 s as the fluid fraction of the flux surface at the outlet goes to zero. Figure 16c shows that some bubbles are ingested under the porous plate during the second parabola, which can also be seen in Figure 16d and e. Looking at the fluid snapshots, outlet gas ingestion appears to occur at t=77 s. However, data shows outlet gas ingestion at 128.0 s. Therefore, the expulsion efficiency range is 88% to 92%, and the lower bound expulsion efficiency is nearly the same as the R/4 baffle plate.

Case 7 – 2.5% Open Area, 400µm, 0.79R, 43.6% Initial Fill

Case 7 compares a 0.79*R upper ring baffle PMD to the base case design R/4 upper ring baffle (Case 3) and the R/3 upper ring baffle (Case 5) at a high initial fill level to determine the effect of larger open area of the 0.79*R plate. As shown in Figure 18, as before, the porous plate and ring baffle traps some of the fluid while the remaining fluid moves upwards to the top of the tank. However, in this case, vapor is ingested during the first upwards-g part of the parabola. Figure 19 shows a constant flow rate except for some small volume errors causing slight variance, up until t=14.0 s where the flow rate goes to near zero due to gas ingestion. Figure 19 also shows that a large volume of bubbles makes it past the porous plate during the upwards-g part of the first parabola. Looking at both the fluid snapshots and the data it can be seen that failure occurs at t=14.0s, shortly after the first parabola begins. Therefore, the expulsion efficiency is 57.7%. However, since this case failed during the first parabola, it is possible that the expulsion efficiency could be even lower. No further cases were run using the 0.79R baffle.

Case 8 – 2.5% Open Area, 800µm, R/4, 19.6% Initial Fill

Case 8 compares a bottom porous plate with 800 micron sized pores with the base case pore size of 400 microns from Case 4 at low fill level. As shown in Figure 20, the porous plate and ring baffle trap some of the fluid while the remaining fluid moves upwards to the top of the tank during the first parabola. From Figure 20b, a small volume of vapor is ingested under the plate during the upwards-g part of the first parabola, but this does not lead to vapor ingestion. Figure 21 indicates gas ingestion around 128 seconds and shows that some bubble ingestion past the porous plate during the upwards-g part of the second parabola. CFD visualization shows that gas ingestion occurs at t=73.0 s. However, the 1D data shows outlet gas ingestion at 128.4 s. Therefore, the expulsion efficiency range is 87.5% to 92.8%. The 800-micron pore size thus leads to a slightly higher (~1%) maximum expulsion efficiency over the 400 micron pore size, but the minimum expulsion efficiency is on the same order.

Case 9 – 0.63% Open Area, 400µm, R/4, 19.6% Initial Fill

Case 9 compares a bottom porous plate with 0.63% open area with the base case open area of 2.5% from Case 4 at low fill level. Results are similar to those of Case 8 in terms of the time of first bubble past the porous plate, vapor ingestion into the outlet (128 s), and expulsion efficiency. From CFD in Figure 22, outlet gas ingestion appears to occur at t=70.5 s. However, data in Figure 23 shows outlet gas ingestion at 128.4 s. Therefore, the expulsion efficiency range is 89-93%.

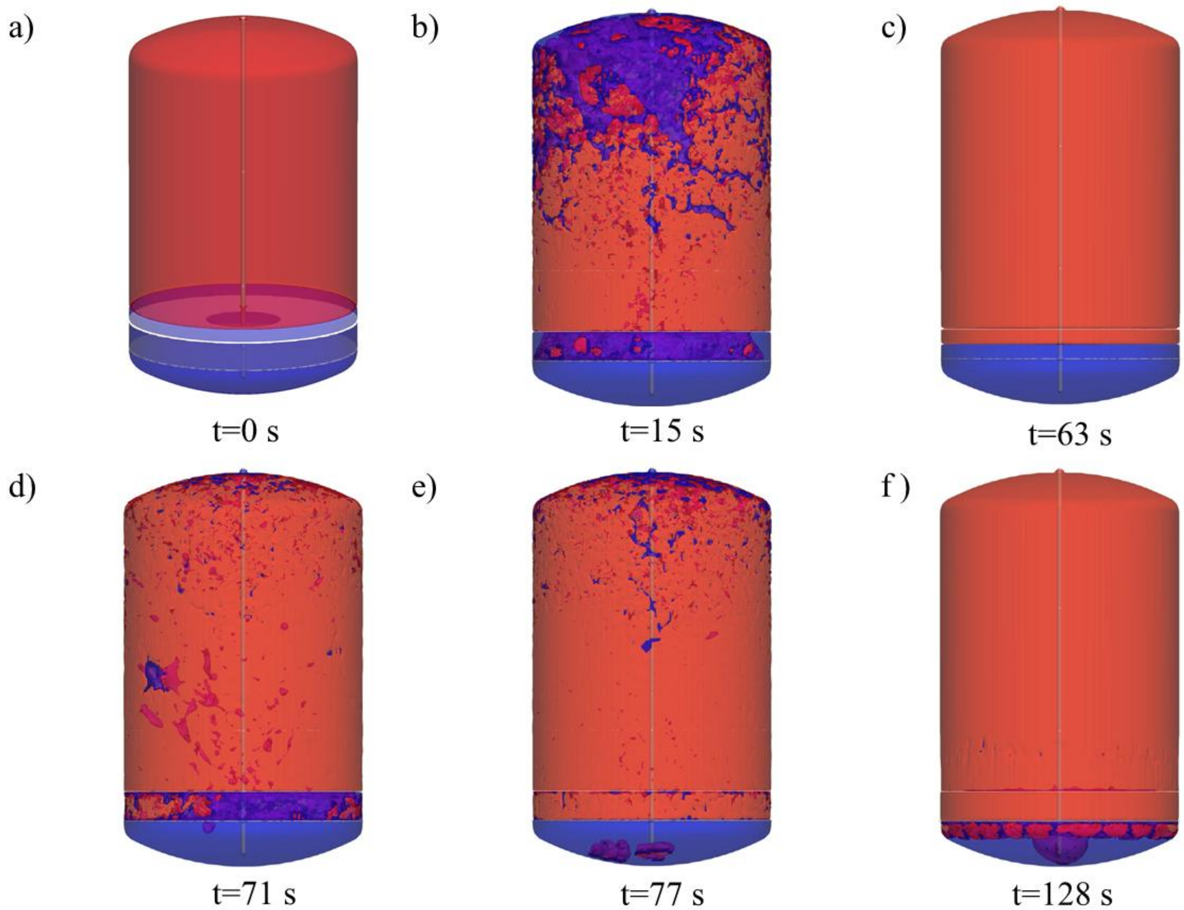

Figure 16: Visualization of Fluid for Case 6 for a) Initial Fill level, b) Middle of First Parabola, c) Before Second Upward-g Parabola, d) First Bubble Ingestion Past Porous Plate, e) First Vapor Ingestion at Outlet, f) Vapor Ingestion According to Outlet Flux Surface Fraction and Sampling Volume Fluid Fraction

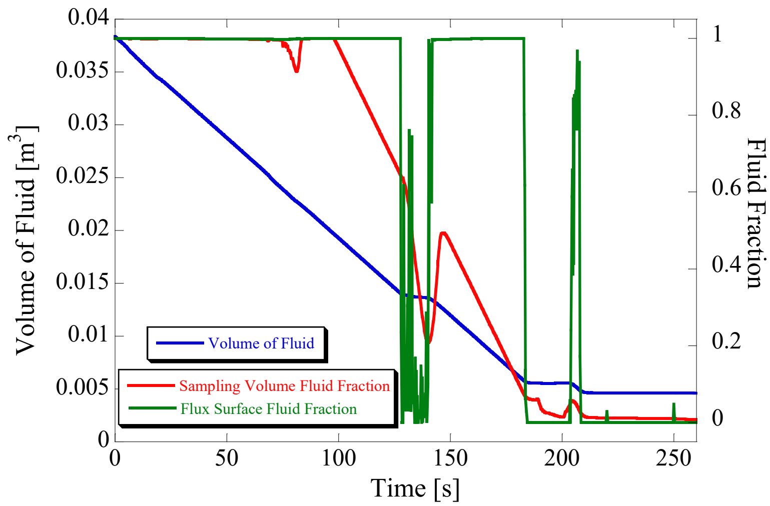

Figure 17: Case 6 – Volume of Fluid, Fluid Fraction of Outlet Flux Surface, and Fluid Fraction of Volume Below Porous Plate vs Time

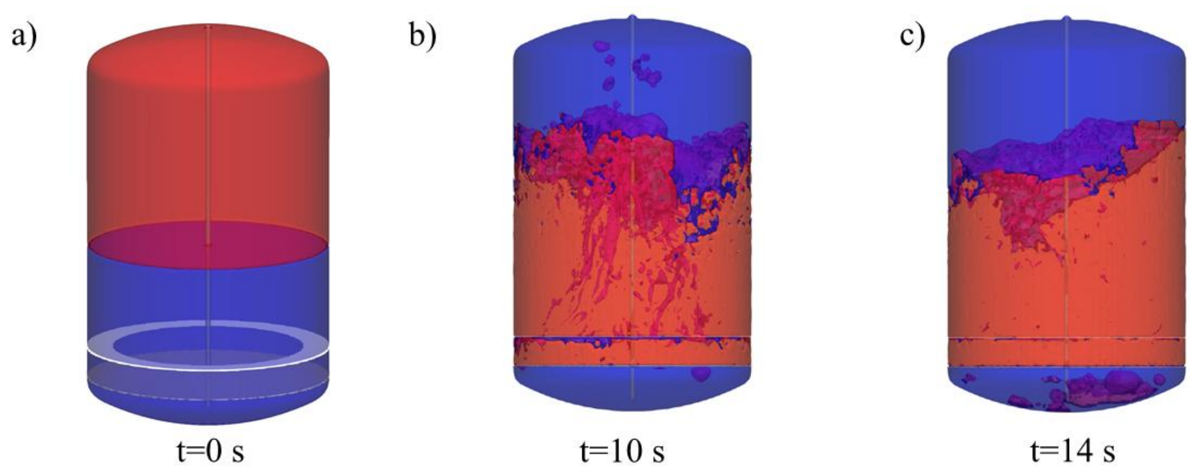

Figure 18: Visualization of Fluid in the Supply Tank as a Function of Time for Case 7 for a) Initial Fill level, b) Instance of First Bubble Ingestion Past Porous Plate, and c) At the Point of Vapor Ingestion

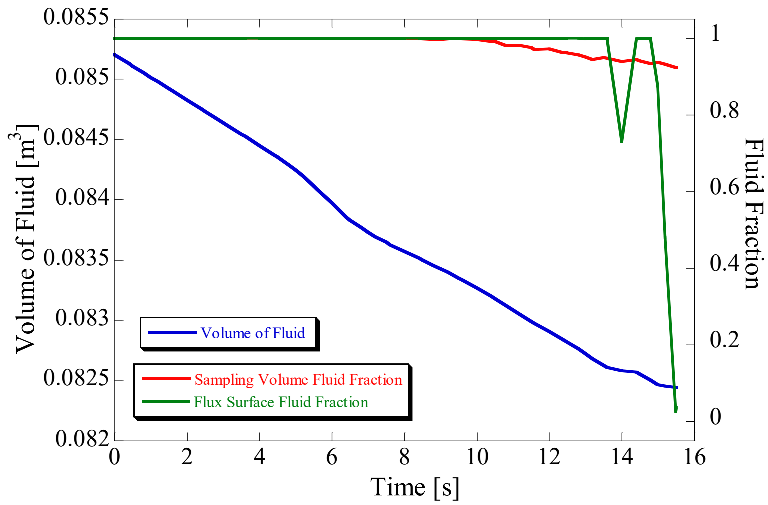

Figure 19: Case 7 – Volume of Fluid, Fluid Fraction of Outlet Flux Surface, and Fluid Fraction of Volume Below Porous Plate vs Time

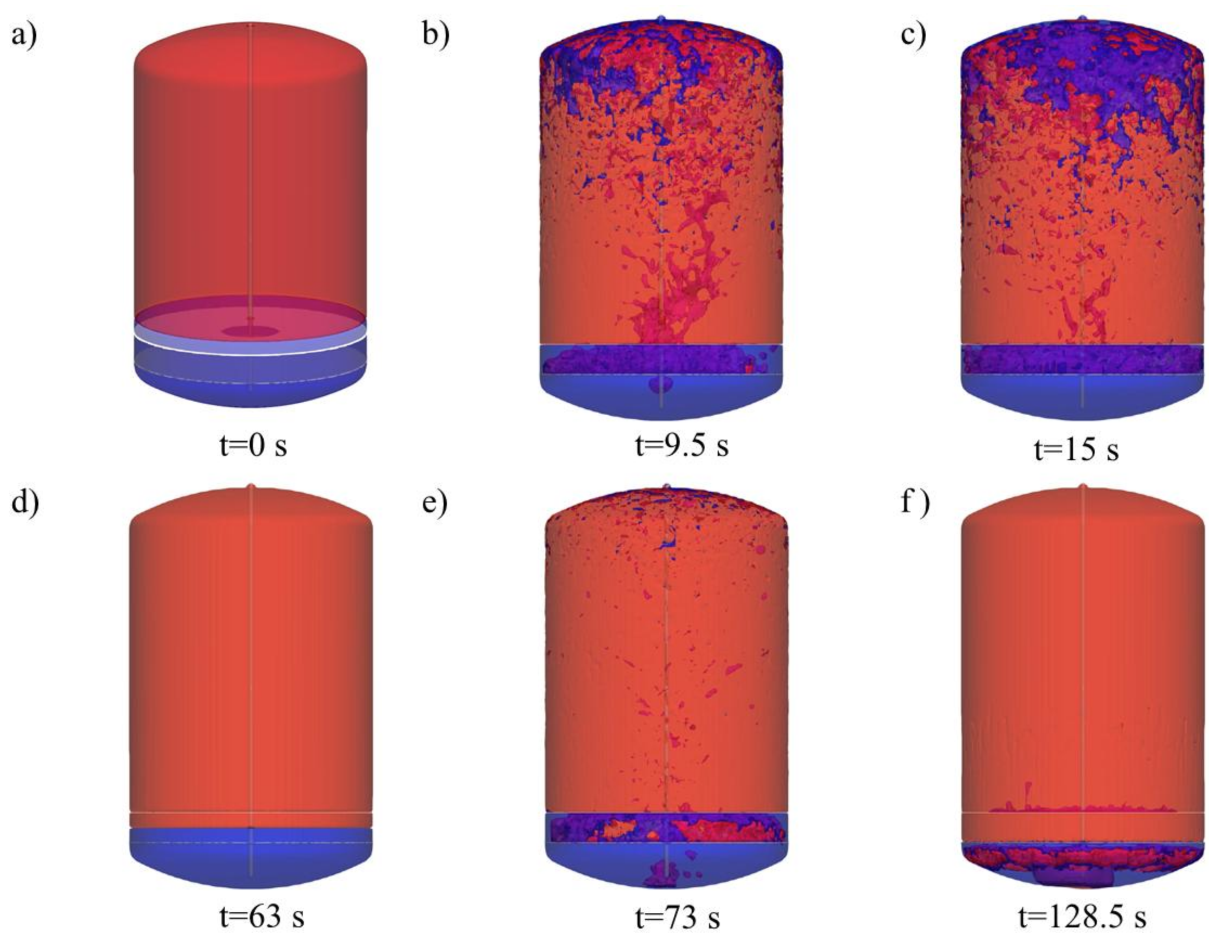

Figure 20: Visualization of Fluid for Case 8 for a) Initial Fill level, b) First Bubble Ingestion Past Porous Plate, and c) During Middle of First Parabola, d) Before Second Upwards-g Parabola, e) First Vapor Ingestion at Outlet, f) Vapor Ingestion According to Outlet Flux Surface Fraction and Sampling Volume Fluid Fraction.

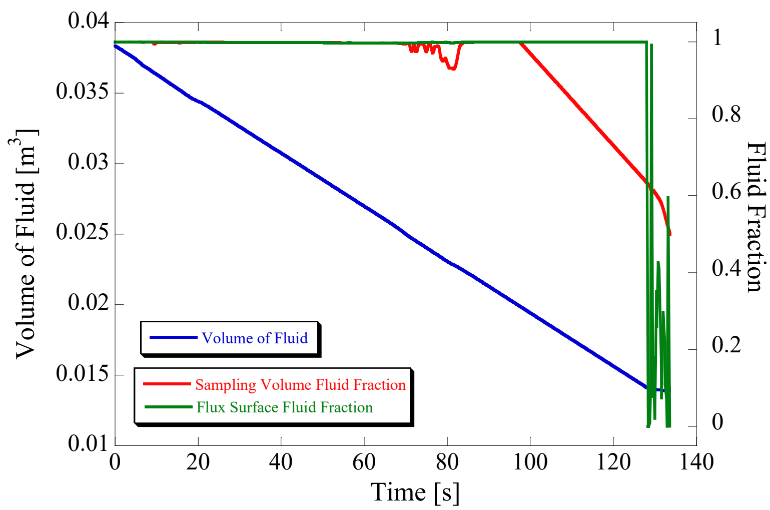

Figure 21: Case 8 – Volume of Fluid, Fluid Fraction of Outlet Flux Surface, and Fluid Fraction of Volume Below Porous Plate vs Time

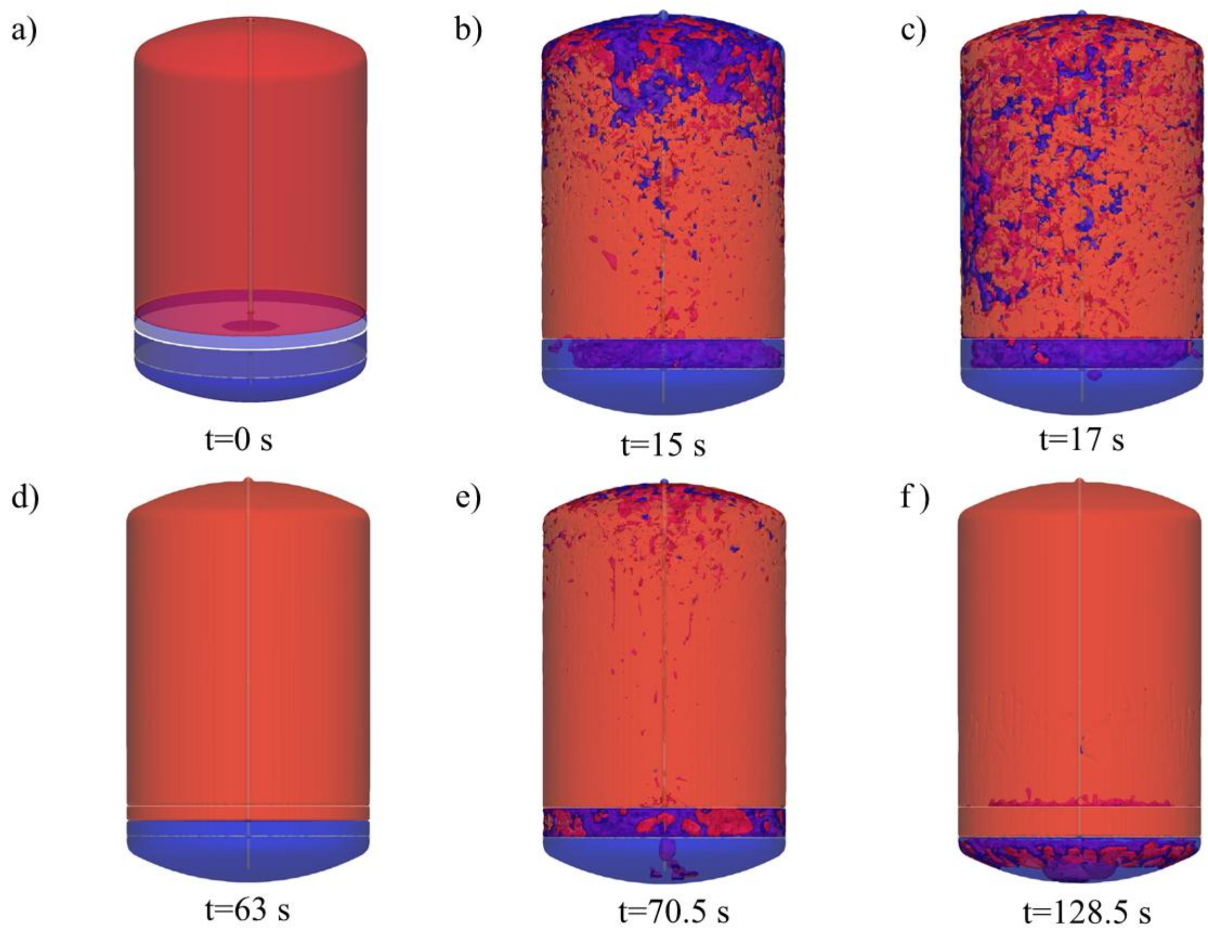

Figure 22: Visualization of Fluid for Case 9 a) Initial Fill level, b) Middle of First Parabola, c) First Bubble Ingestion Past Porous Plate, d) Before Second Upwards-g Parabola, e) First Vapor Ingestion at Outlet, f) Vapor Ingestion According to Outlet Flux Surface Fraction and Sampling Volume Fluid Fraction.

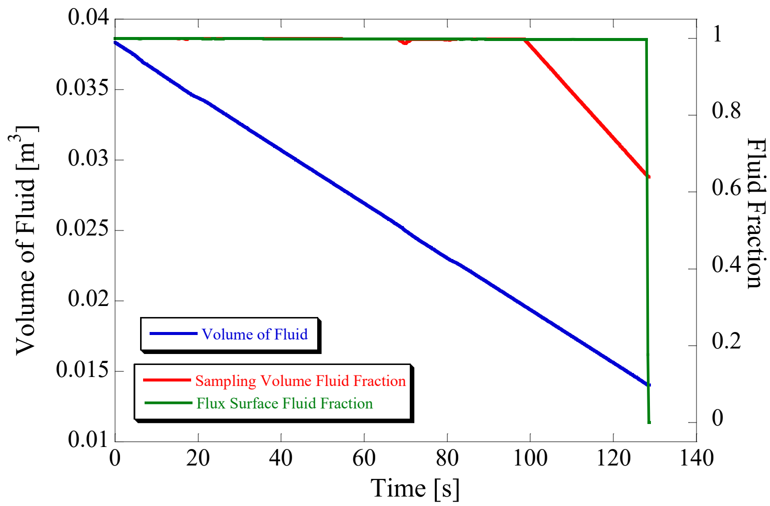

Figure 23: Case 9 – Volume of Fluid, Fluid Fraction of Outlet Flux Surface, and Fluid Fraction of Volume Below Porous Plate vs Time

Case 10 – Double 1.27 cm Plate, Low Magnitude Gravity, 17.0% Initial Fill

Cases 6, 8, and 9 all yielded similar expulsion efficiency implying that independently changing the pore size smaller or decreasing the open area percentage of the bottom porous plate yielded no noticeable impact on expulsion efficiency. However, the pressure drop across the plate was obviously different. Changing the opening area on the top plate has impacted results the most, since the R/3 plate and R/4 baffle plates yielded at least 29-35% higher expulsion efficiency over the 0.79R plate. This indicates that having lower open area is preferred for the top plate. Instead of spending further time attempting to optimize the opening on the top baffle, it was decided to replace the ring baffle with a second porous plate to improve liquid communication with the top of the bottom porous plate.

At first, the thickness of both porous plates was adjusted to 1.27 cm due to structural concerns from finite element analysis calculations. The open area for both plates was chosen to be 0.63% due to structural concerns. A pore size of 400 μm was used for both plates. With these design parameters set, new simulations were run to determine the expulsion efficiency of the new design.

Figure 24 plots the first simulation for the double porous plate, at the nominal lower gravity level, as a sanity check of the design. As shown, the double porous plates are able to maintain liquid below both of the plates. Figure 25 shows a constant flow rate throughout the whole simulation indicating no vapor ingestion at the outlet. Additionally, the fluid filled area of the flux surface does not drop, and no bubbles make it past the lower porous plate throughout the simulation. This simulation was not run until breakdown, so no expulsion efficiency was computed.

Case 11 – Double 1.27 cm Plate, 9.1% Initial Fill

Case 11 was another sanity check on the design and compares with Case 10, but at worst-case higher gravity level and slightly lower fill level. As shown in Figure 26, the upper porous plate is able to prevent liquid from passing upwards to the top of the tank during the upwards acceleration and therefore able to maintain communication between liquid and the top of the bottom porous plate. Figure 27a shows a constant flow rate throughout the simulation run which indicates vapor is not being ingested. Figure 27b and 27c substantiate this finding with no change in fluid fraction at the outlet flux surface or sampling volume fraction. This simulation was not run until breakdown, so no expulsion efficiency was computed, but based on the fill level at the end of the simulation, the expulsion efficiency had to be >91.7%.

Case 12 – Double 1.27 cm Plate, 13.3% Initial Fill

Case 12 employs the double plate PMD initialized at a lower fill level, but in worst-case higher gravity and at a higher fill level than Case 11 to determine the residuals at breakdown. As shown in Figure 28, the double porous plates are able to trap all of the liquid below both of the plates during low-g during the first parabola. Vapor is eventually ingested below the second plate during the second parabola as shown in Figure 28d, with vapor ingestion into the outlet shortly thereafter. Figure 29 indicates vapor ingestion around 67s. Comparing this with fluid snapshots predicted breakdown of t = 67.4 s, the expulsion efficiency compares well between the two cases at 93.2%.

Case 13 – Double 0.953 cm Plate, 9.1% Initial Fill

Case 13 compares thinner 0.953 cm double plates with the thicker 1.27 cm plates at the same initial fill level and gravity level from Case 11. Similar to Case 11, Case 13 was run as a sanity check on the design. Similar results are shown between the two cases in terms of resistance to bubble ingestion comparing Figures 26 and 30. Figure 31 shows no evidence of bubble ingestion over the simulation time. This simulation was not run until breakdown, but based on the fill level at the end of the simulation, the expulsion efficiency is > 92%.

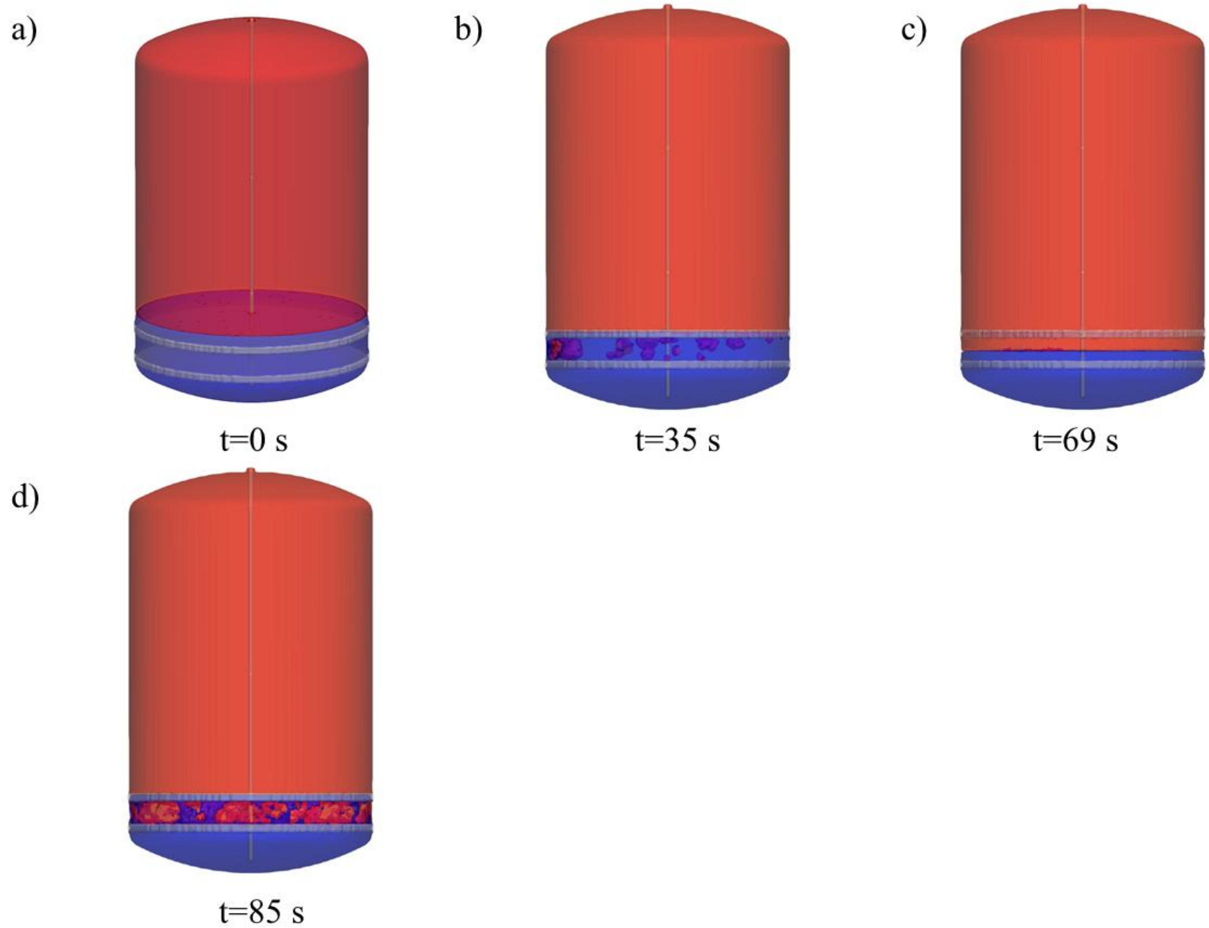

Figure 24: Visualization of Fluid for Case 10 a) Initial Fill level, b) During Middle of First Parabola, c) Before Second Upwards-g Parabola, and d) During Middle of Second Parabola

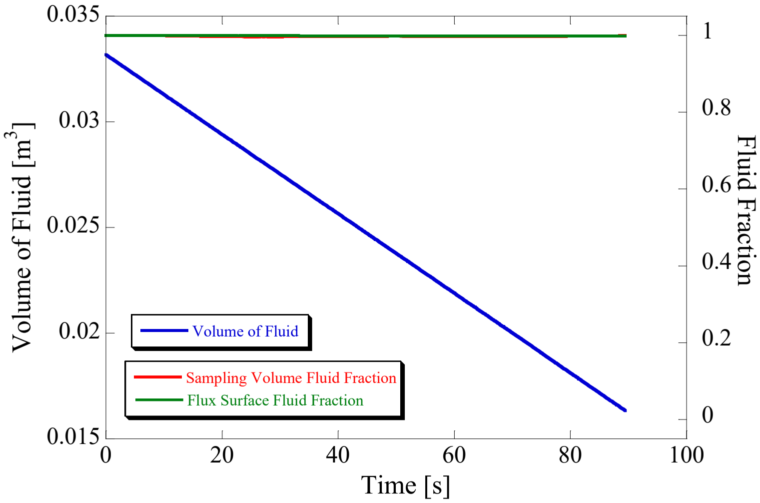

Figure 25: Case 10 – Volume of Fluid, Fluid Fraction of Outlet Flux Surface, and Fluid Fraction of Volume Below Porous Plate vs Time

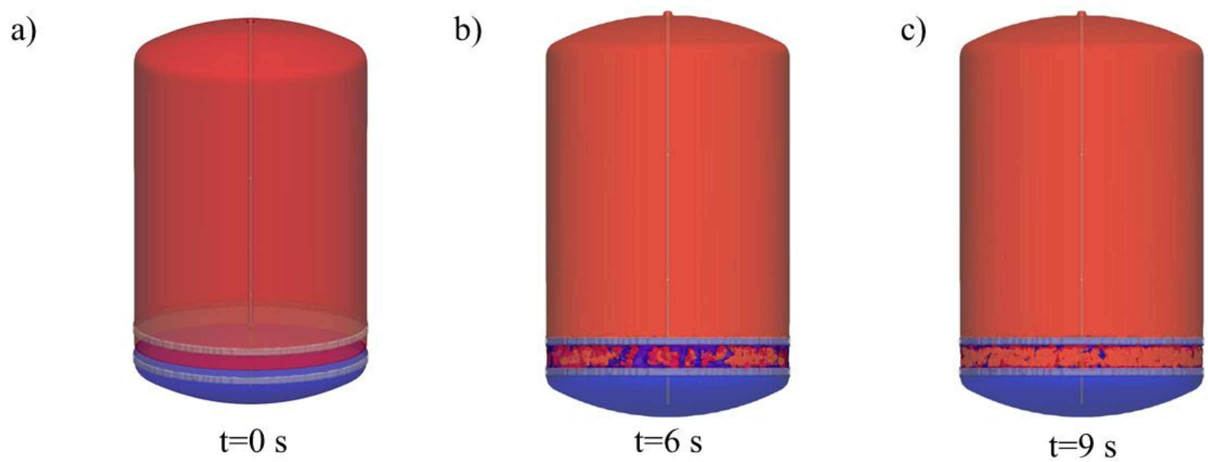

Figure 26: Visualization of Fluid for Case 11 a) Initial Fill level, b) During Start of First Upwards-g Parabola, and c) First Configuration at End of Simulation

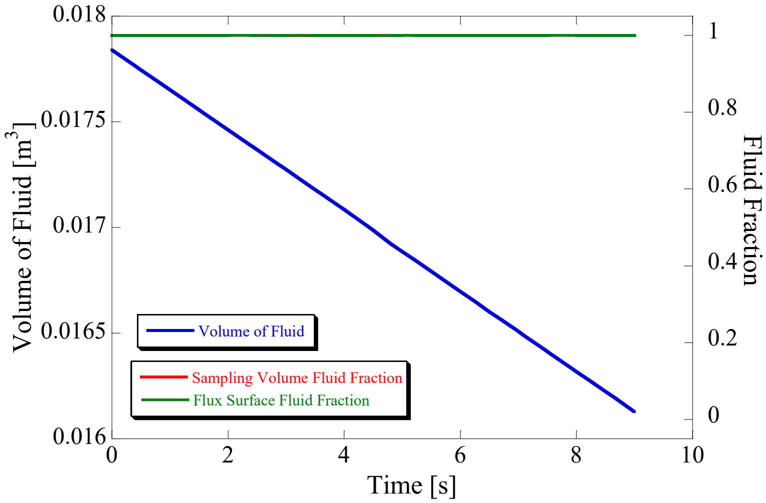

Figure 27: Case 11 – Volume of Fluid, Fluid Fraction of Outlet Flux Surface, and Fluid Fraction of Volume Below Porous Plate vs Time

Simulations Overview

Table 3 presents a summary of all the simulations. The measured and calculated pressure drop across the plate are tabulated to compare FLOW-3D with [36]. Three times are indicated for most of the runs: first bubble past the bottom porous plate from CFD visualization, visual vapor ingestion at the outlet via CFD, and indication of vapor ingestion via the 1D data. Also listed is the fill level at breakdown via CFD and 1D data, and the minimum expulsion efficiency between the CFD and data.

Results are summarized as follows: First and most importantly, any slight off-nominal change in the gravity profile onboard the plane would result in significantly higher residuals in the tank, minimizing the total experimental run time for a cryogenic fluid-based payload, because without a PMD inside the tank at the higher gravity level, vapor ingestion occurs at the first parabola. While not shown here, simulations were run at intermediate gravity levels with the same fate of premature breakdown. Second, the measured and calculated pressure drop across the bottom porous plate for each case are relatively close for all of the cases, essentially validating the Flow-3D pressure drop model. Third, changing the pore size within the tolerable range had negligible impact on expulsion efficiency and flow-through-screen resistance. Fourth, the open area percentage had a negligible impact on expulsion efficiency (over the range of open area percentages modeled), but did affect the flow-through-screen resistance. Fifth, the open area of the top baffle plate had a major impact on expulsion efficiency, so the design shifted to a double plate configuration. Sixth and finally, the expulsion efficiency did not vary with the thickness of the plates.

Results show consistently higher expulsion efficiency between the CFD visualization and 1D data using the double plate configuration. From FEA calculations it was also determined that the thickness of both plates could be safely lowered to 0.953 cm to reduce the overall mass of the PMD. The final design is thus the 0.63% open area, 0.953 cm thick, 400-micron pore sized double plate configuration.

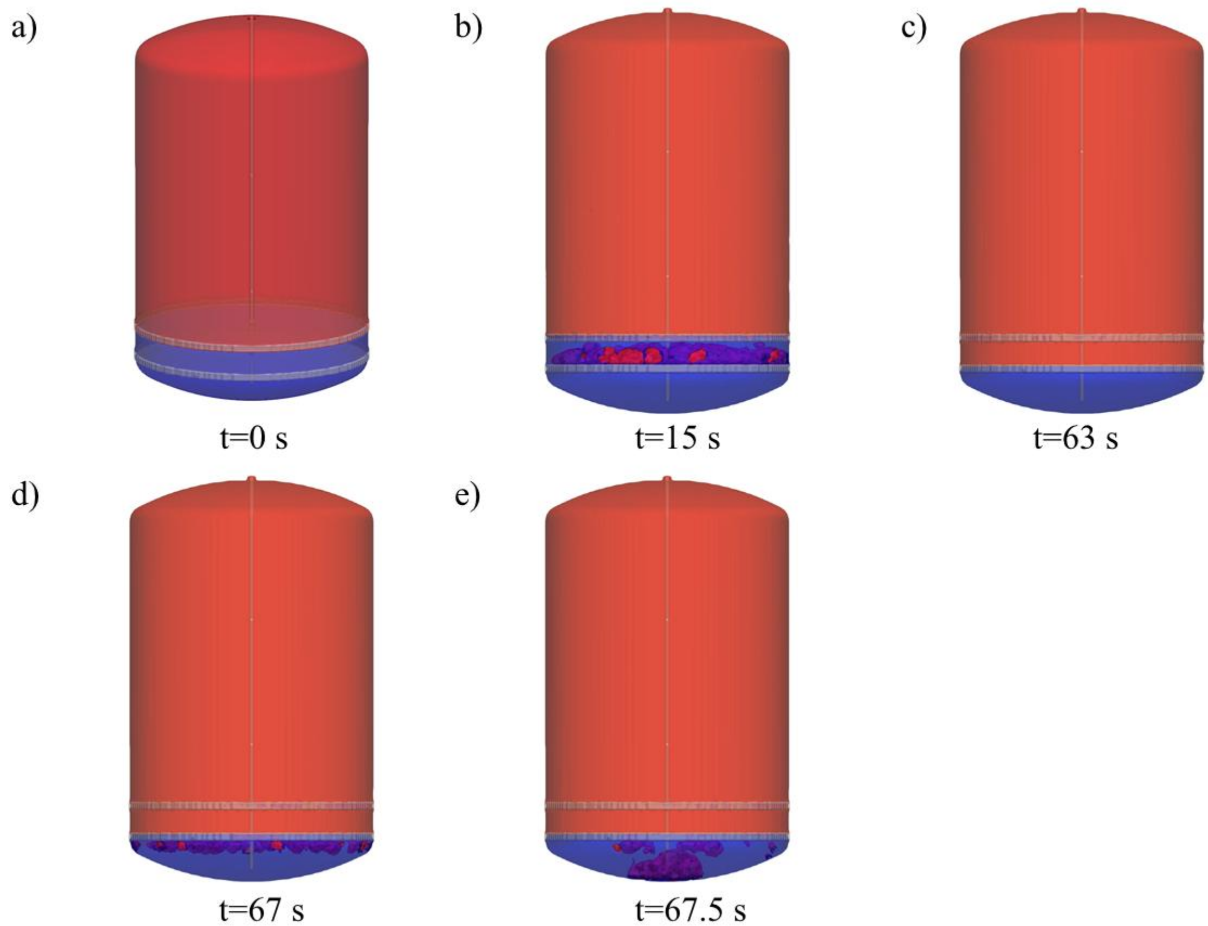

Figure 28: Visualization of Fluid for Case 12 a) Initial Fill level, b) During Middle of First Parabola, c) Before Second Upwards-g Parabola, d) First Bubble Ingestion Past Porous Plate, e) Vapor Ingestion at Outlet, and f) Vapor Ingestion According to Outlet Flux Surface Fraction and Sampling Volume Fluid Fraction

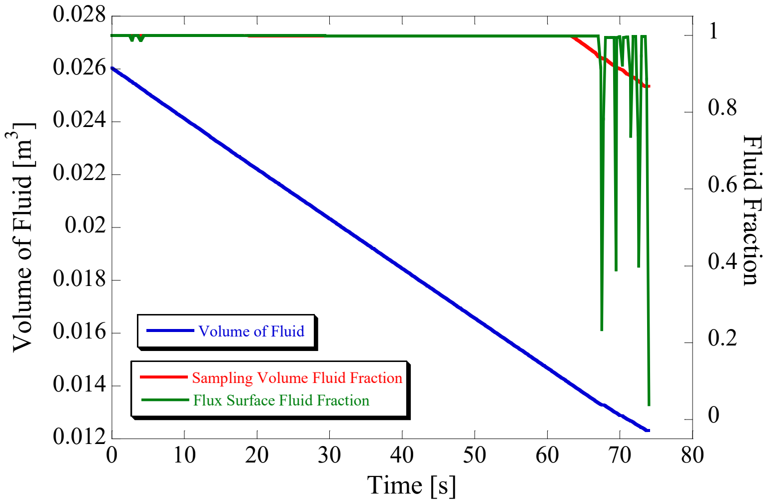

Figure 29: Case 12 – Volume of Fluid, Fluid Fraction of Outlet Flux Surface, and Fluid Fraction of Volume Below Porous Plate vs Time

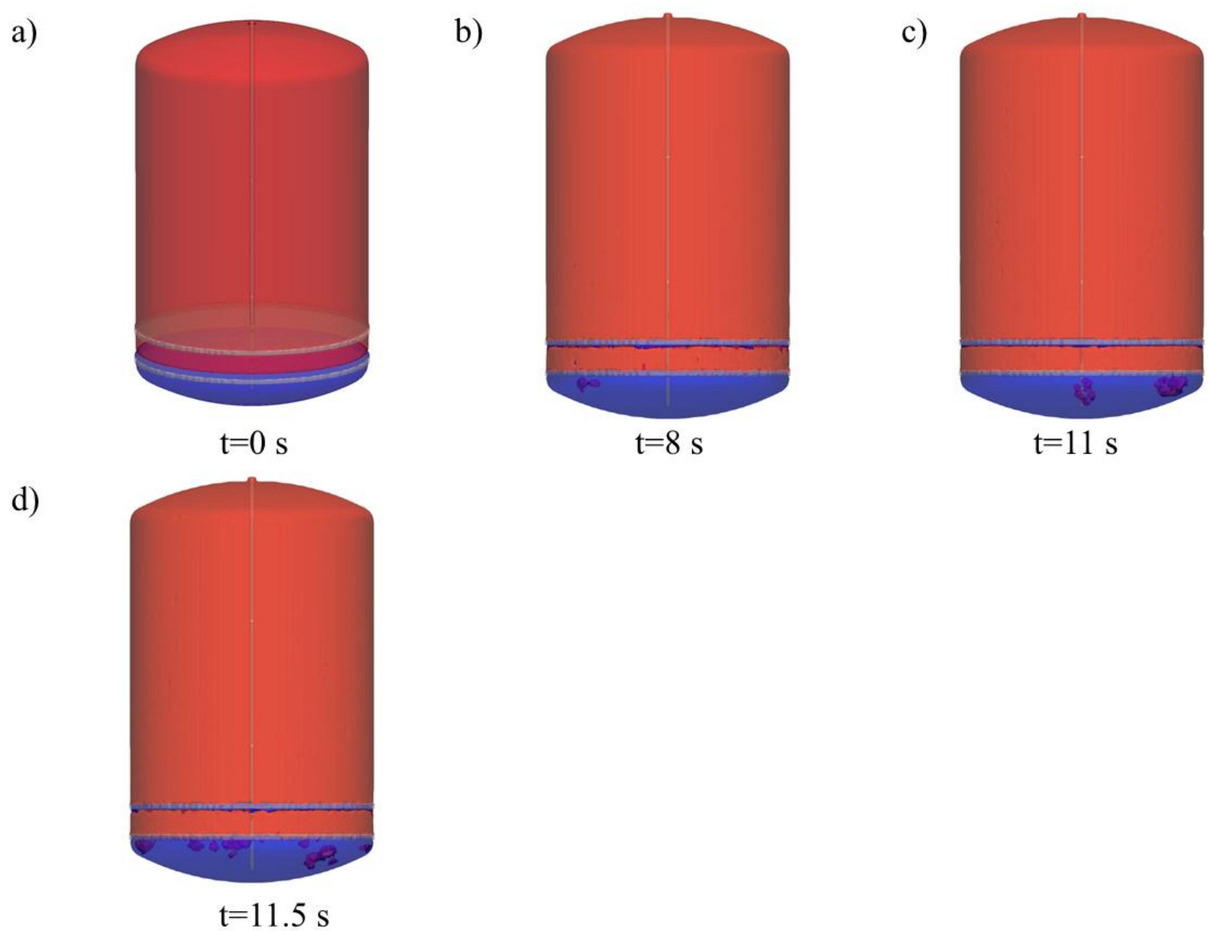

Figure 30: Visualization of Fluid for Case 13 a) Initial Fill level, b) First Bubble Ingestion Past Porous Plate, c) First Visualization of Vapor Near the Outlet, and f) End of Simulation.

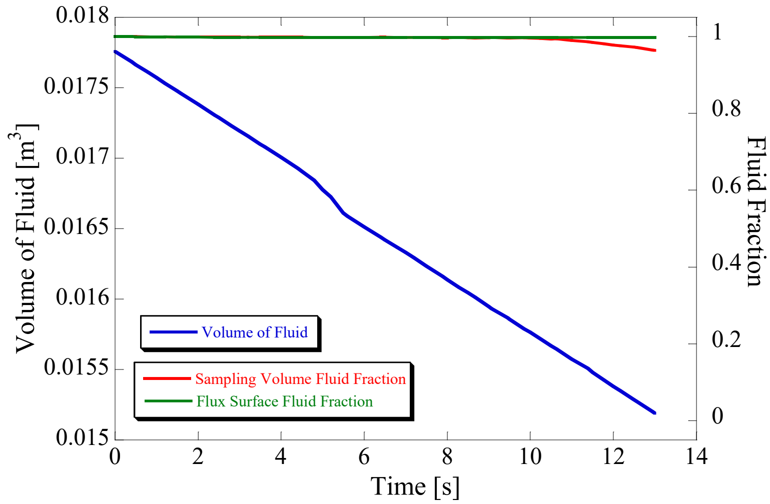

Figure 31: Case 13 – Volume of Fluid, Fluid Fraction of Outlet Flux Surface, and Fluid Fraction of Volume Below Porous Plate vs Time

Table 3: Summary of Simulation Results

Case #	Description	Measured Pressure Drop across Bottom Plate [Pa]	Calculated Pressure Drop across Bottom Plate [Pa]	Visual Failure Fill Level [%]	Data Failure Fill Level [%]	Minimum Expulsion Efficiency [%]
1	No PMD, Lower Gravity	-	-	6.9	6.9	92
2	No PMD, Higher Gravity	-	-	98.6	98.6	1.4
3	2.5% OA, 400um, R/4, 57.7% Fill	1.22	1.11	-	-	-

4	2.5% OA, 400um, R/4, 19.6% Fill	1.05	1.11	12.6	12.6	87.4
5	2.5% OA, 400um, R/3, 48.4% Fill	1.19	1.11	-	-	-
6	2.5% OA, 400um, R/3, 19.6% Fill	1.05	1.11	12	7.2	88
7	2.5% OA, 400um, 0.79R, 43.6% Fill	0.937	1.11	42.3	42.3	57.7
8	2.5% OA, 800um, R/4, 19.6% Fill	0.964	1.03	12.5	7.2	87.5
9	0.63% OA, 400um, R/4, 19.6% Fill	18.8	16.3	10	7.2	90
10	Double 1.27 cm Plate, Lower Gravity, 17.0% Fill	18.6	16.3	-	-	-
11	Double 1.27 cm Plate, 9.1% Fill	18.6	16.3	-	-	-
12	Double 1.27cm Plate, 13.3% Fill	19	16.3	6.8	6.8	93.2

13	Double 0.953 cm Plate, 9.1% Fill	15.7	16.3	-	-	-

V. Model Validation

The most appropriate way to validate a PMD design is to determine the expulsion efficiency of the particular design and compare with model results. The same PMD design was recently installed into a scaled down (by tank radius) supply tank onboard a series of parabolic flights. For these flights, the requirement was constant mass flow rate out of the tank during both zero-g and hypergravity. Results are plotted in Figure 32 for three flight experiments where residual volume was determined from a "burn-time" integration mass gauging method. Table 4 shows the differences in the flight experiments in terms of mass flow rate, gravity level at the point of breakdown, and expulsion efficiency. As shown, the residual liquid volume inside the tank nearly perfectly linearly decreases with time up to the point of vapor ingestion in the transfer line.

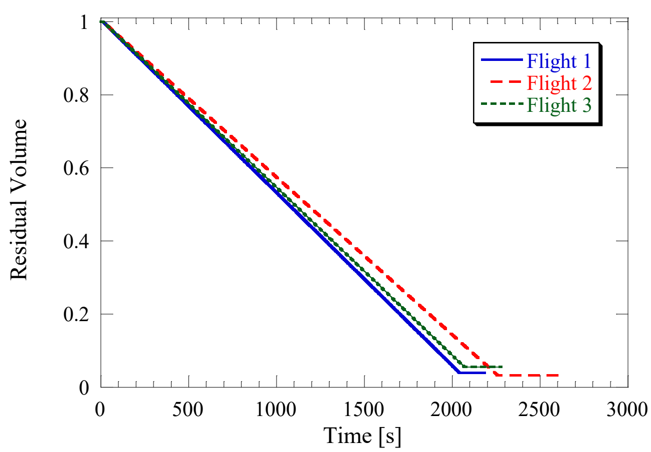

Figure 32: Residual Volume of Liquid in the Storage Tank as a Function of Time

Table 4: Summary of Results

Flight #	**Mass Flow Rate [kg/s]**	**Negative-g Level at Breakdown [m/s^2]**	**Expulsion Efficiency [%]**
1	0.061	0.211	96.1
2	0.055	0.243	96.7
3	0.059	0.912	94.7

Trends are as follows: First, comparing flights 1 and 3 at similar flow rates, the expulsion efficiency at the higher negative-g level is noticeably lower than the lower negative-g level by 1.5% of the volume of the tank. Second, comparing flights 1 and 2, for similar negative g-levels, the lower flow rate promotes lower residuals in the tank at breakdown, as expected. Third and most importantly, the experimentally determined expulsion efficiencies are all slightly better than the predicted values at similar conditions.

VI. Conclusion

There is a need for reduced gravity data for various gravity-dependent cryogenic fluid management (CFM) technologies, including pressurization, line and tank chilldown and fill, and propellant management devices. Parabolic flights onboard the ZeroG aircraft offer generous size, weight, and power for payloads, offer 30 parabolas of 17-20 seconds of microgravity per flight, and allow cryogenic nitrogen onboard the aircraft, all at a cost-efficient price. Parabolic flights have recently been used to acquire needed CFM data with a high degree of success, yielding improved understanding of fundamental physics and predictive capability. In order to maximize the collection of low-g data during future cryogenic parabolic flights, it is required to extract as much liquid as possible from the supply tank, despite variable gravity levels between microgravity and hypergravity. Given that the maximum negative gravity levels during flights can vary by a factor of 4, premature vapor ingestion into the tank outlet is guaranteed without the presence of a PMD.

This paper presented design and VOF CFD simulations of the fluid motion inside a propellant tank onboard a parabolic flight and subsequent design of the first known bi-directional cryogenic PMD for a parabolic flight. The goal of the study was to obtain a design that yielded an expulsion efficiency of >90% to maximize science for the payload in the worst-case gravitational environment. A parametric study was conducted on the effects of the ring baffle size, and the plate porosity, pore size, and thickness. CFD simulations were performed using FLOW-3D to determine the flow characteristics, pressure drop, and expulsion efficiency of the varying PMD designs. Based on results, a double porous plate PMD was designed that exceeded the desired expulsion efficiency. This design has already been implemented into an upcoming cryogenic parabolic flight experiment and can easily be scaled to different sized tanks. This design was recently implemented into a slightly smaller scaled cryogenic storage tank and comparison between the model predicted expulsion efficiency with the experimentally determined expulsion efficiency clearly shows the design exceeds performance expectations.

Acknowledgments

This work was funded by the Reduced Gravity Cryogenic Transfer Project under the Space Technology Mission Directorate at NASA Glenn Research Center. The authors wish to acknowledge the following individuals who positively contributed to this work: Eric Carlberg, Sam Darr, Jesse DeFiebre, Bryan Fraser, Dr. Mohammad Kassemi, David Koci, Alok Majumdar, Mariano Mercado, Erin Tesny, Steve Willming and the support staff at Flow3D.

References

[1] Hartwig, J.W. "Liquid Acquisition Devices for Advanced In-Space Cryogenic Propulsion Systems" Elsevier: Boston, MA, November, 2015.

[2] Hartwig, J.W. "Propellant Management Devices for Low Gravity Fluid Management: Past, Present, and Future Applications" *AIAA Journal of Spacecraft and Rockets* Vol. 54, No. 4, 2017, pp. 808 – 824. https://doi.org/10.2514/1.A33750

[3] Darr, S.R., Dong, J., Glikin, N., Hartwig, J.W., Majumdar, A., LeClair, A., and Chung, J.N. "Effect of Gravity on Cryogenic Flow Boiling and Chilldown" *Nature Microgravity* vol. 2, 2016, pp. 16033. https://doi.org/10.1038/npjmgrav.2016.33

[4] Chung, J.N., Dong, J., Wang, H., Darr, S.R., and Hartwig, J.W. "An Advance in Transfer Line Chilldown Heat Transfer of Cryogenic Propellants in Microgravity using Microfilm Coatings for Enabling Deep Space Explorations" *Nature Microgravity* vol. 7, no. 21, 2021. https://doi.org/10.1038/s41526-021-00149-5

[5] Hartwig, J.W., Chung, J.N., Dong, J., Han, B., Wang, H., Darr, S.R., Taliaferro, M., Jain, S., and Doherty, M. "Cryogenic Nitrogen Flow Boiling and Chilldown Experiments in Microgravity using Pulse Flow and Low Thermally Conductive Coatings" *Nature Microgravity* 2022. https://doi.org/10.1038/s41526-022-00220-9

[6] https://www.gozerog.com/

[7] Clark, J. and Hartwig, J.W. "Assessment of Prediction and Efficiency Parameters for Cryogenic No-Vent Fill" *Cryogenics* 117, 103309. 2021. https://doi.org/10.1016/j.cryogenics.2021.103309

[8] Ganesan, V., Patel, R., Hartwig, J.W., and Mudawar, I. "Universal Critical Heat Flux (CHF) Correlations for Cryogenic Flow Boiling in Uniformly Heated Tubes" *International Journal of Heat and Mass Transfer* 166, 120678. 2021. https://doi.org/10.1016/j.ijheatmasstransfer.2020.120678

[9] Ganesan, V., Patel, R., Hartwig, J.W., and Mudawar, I. "Review of Databases and Correlations for Saturated Flow Boiling Heat Transfer Coefficient for Cryogens in Uniformly Heated Tubes, and Development of New Consolidated Database and Universal Correlations" *International Journal of Heat and Mass Transfer* 179. 121656. 2021. https://doi.org/10.1016/j.ijheatmasstransfer.2021.121656

[10] Ganesan, V., Patel, R., Hartwig, J.W., and Mudawar, I. "Universal Correlations for Post-CHF Saturated and Superheated Flow Film Boiling Heat Transfer Coefficient, Minimum Heat Flux and Rewet Temperature for Cryogenic Fluids in Uniformly Heated Tubes" *International Journal of Heat and Mass Transfer* 195, 123054. 2022. https://doi.org/10.1016/j.ijheatmasstransfer.2022.123054

[11] Tesny, E., Hauser, D., and Hartwig, J.W. "Tank Sizing Analysis for the Reduced Gravity Cryogenic Transfer Receiver Tank" *2021 TFAWS Conference* August 24 – 26, 2021.

[12] Majumdar, A., LeClair, A., Martin, A., Rhys, N., and Hartwig, J.W. "Numerical Modeling of No Vent Fill of a Cryogenic Tank" *AIAA-2020-3797, 2020 Joint Propulsion Conference* New Orleans, LA, August 24 – 26, 2020. https://doi.org/10.2514/6.2020-3797

[13] Majumdar, A., LeClair, A., Hartwig, J.W., and Ghiaasiaan, M. "Numerical Modeling of No Vent Filling of a Cryogenic Tank with Thermodynamic Vent System Augmented Injector" *Cryogenics* 131, 103651. 2022. https://doi.org/10.1016/j.cryogenics.2023.103651

[14] White, D. "FLUENT Conjugate Heat Transfer Simulations of K-Site LH_2 Tank Chilldown" *RGCT-DOC-FY20-03*, June 19, 2020.

[15] Flow Science, Inc., Santa Fe, NM, USA. FLOW-3D® Version 12.0, 2019.

[16] Sicilian, J.M. and Hirt, C.W., "Numerical Simulation of Propellant Sloshing for Spacecraft," American Society of Mechanical Engineers Winter Annual Meeting, December 9-14, 1984.

[17] Eastes, T.W., Chang, Y.M., Hirt, C.W., and Sicilian, J.M., "Zero-Gravity Slosh Analysis," American Society of Mechanical Engineers Winter Annual Meeting, November, 1985.

[18] Navickas, J., Cross, C.R., and Van Winkle, D.D., "Propellant Tank Forces Resulting from Fluid Motion in a Low-Gravity Field," American Society of Mechanical Engineers Symposium in Microgravity Fluid Mechanics, Winter Annual Meeting, Anaheim, CA, December 7-12, 1986.

[19] Martin, R.E., “Effects of Transient Propellant Dynamics on Deployment of Large Liquid Stages in Zero-Gravity with Application to Shuttle-Centaur,” Acta Astronautical, Vol. 15, No. 6/7, 1987, pp. 331-340. https://doi.org/10.1016/0094-5765(87)90168-8

[20] Der, J,J, and Stevens, C.L., “Low-Gravity Bubble Reorientation in Liquid Propellant Tanks,” AIAA Paper 87-0622, January 1987. https://doi.org/10.2514/6.1987-622

[21] Fisher, M.F., Schmidt, G.R., and Martin, J.J., “Analysis of Cryogenic Propellant Behavior in Microgravity and Low Thrust Environments”, 27th AIAA Joint Propulsion Conference, June, 1991. https://doi.org/10.1016/0011-2275(92)90272-C

[22] Sasmal, G.P., Hochstein, J.I., and Wendl, M.C., “Computational Modeling of the Pressurization Process in a NASP Vehicle Propellant Tank Experimental Simulation,” AIAA Paper 91-2407, June, 1991. https://doi.org/10.2514/6.1991-2407

[23] Letourneur, Y., and Sicilian, J., “Propellant Reorientation Effects on the Attitude of the Main Cryotechnic Stage of Ariane V,” AIAA Paper 93-2081, June, 1993. https://doi.org/10.2514/6.1993-2081

[24] Grayson, G.D. and Navickas, J., “Interaction Between Fluid-Dynamic and Thermodynamic Phenomena in a Cryogenic Upper Stage,” AIAA Paper 93-2753, July, 1993. https://doi.org/10.2514/6.1993-2753

[25] Figus, C. and Ounougha, L., “Correlations between Neutral Buoyancy Tests and CFD,” ESASP-465, Spacecraft Propulsion, Third International Conference, Cannes, FR, October 10 – 13, 2000.

[26] Grayson, G.D., Lopez, A., Chandler, F.O., Hastings, L.J., and Tucker, S.P. “Cryogenic Tank Modeling for the Saturn AS-203 Experiment,” AIAA Paper 2006-5258, July, 2006. https://doi.org/10.2514/6.2006-5258

[27] Navickas, J. and Cheng, P.Y., “Effect of Propellant Sloshing on the Design of Space Vehicle Propellant Storage Systems,” AIAA Paper 90-2006, July, 2006. https://doi.org/10.2514/6.1990-2006

[28] Bakkum, A., Schultz, K., Braun, et al., “Investigation of Propellant Sloshing and Zero Gravity Equilibrium for the Orion Service Module Propellant Tanks, Wisconsin Space Conference,” 20th Annual Wisconsin Space Conference, Green Bay, WI, August 19 – 20, 2010.

[29] Behruzi, P., Klatte, J., Fries, N., et al., “Cryogenic Propellant Management Sounding Rocket Experiments on TEXUS 48,” AIAA Paper 2013-3904, July, 2013. https://doi.org/10.2514/6.2013-3904

[30] Gaulke, D. and Dreyer, M.E., “CFD Simulation of Capillary Transport of Liquid Between Parallel Perforated Plates using FLOW-3D,” Microgravity Science and Technology, vol. 27, 2015, pp. 261 – 271. https://doi.org/10.1007/s12217-015-9449-6

[31] Konopka, M., Noeding, P., Klatte, J., et al., “Analysis of LN2 Filling, Draining, Stratification and Sloshing Experiments,” AIAA Paper 2016-4272, June, 2016. https://doi.org/10.2514/6.2016-4272

[32] Manning, R.E., Ballinger, I., Bhatia, M., and Dowdy, M., “Design of the Europa Clipper Propellant Management Device,” AIAA Paper 2019-3858, August, 2019. https://doi.org/10.2514/6.2019-3858

[33] Lemmon, E.W., Bell, I.H., Huber, M.L., McLinden, M.O. NIST Standard Reference Database 23: Reference Fluid Thermodynamic and Transport Properties-REFPROP, Version 10.0, National Institute of Standards and Technology, Standard Reference Data Program, Gaithersburg, 2018.

[34] Flow Science, Inc., Santa Fe, NM, USA. FLOW-3D® Version 12.0 User Manual, 2019.